Multicore Magnetic Particles: Synthesis and Characterization of Magneto-Structural Properties

Lenka Vítková

Bachelor's thesis
2017

Tomas Bata University in Zlín
Faculty of Technology

Univerzita Tomáše Bati ve Zlíně

Fakulta technologická

Ústav fyziky a mater. inženýrství

akademický rok: 2016/2017

ZADÁNÍ BAKALÁŘSKÉ PRÁCE
(PROJEKTU, UMĚLECKÉHO DÍLA, UMĚLECKÉHO VÝKONU)

Jméno a příjmení:	**Lenka Vítková**
Osobní číslo:	**T14381**
Studijní program:	**B2808 Chemie a technologie materiálů**
Studijní obor:	**Materiálové inženýrství**
Forma studia:	**prezenční**
Téma práce:	**Vícejaderné magnetické částice: syntéza a charakterizace magneto-strukturálních vlastností**

Zásady pro vypracování:

1. The student should perform the literature review on the magnetic iron oxide nanoparticles properties and application for magnetic hyperthermia cancer treatment. Multicore magnetic particles, their properties, ways of synthesis and advantages over single-core nanoparticles should be considered in more details. The literature sources used should be cited in a proper way.

2. The student should get the experience in chemical laboratory work, methods of magnetic particles synthesis and characterization of their magneto-structural properties.

3. The student should perform the synthesis of samples of multicore magnetic particles with different morphology and magnetic interaction between them and correlate the synthesis parameters, properties of the dispersion medium with the magneto-structural properties of particles and their heating efficiency in alternating magnetic field.

4. The student should present the obtained results in a proper way and perform their discussion.

Rozsah bakalářské práce:

Rozsah příloh:

Forma zpracování bakalářské práce: **tištěná**

Seznam odborné literatury:

1. **R.M. Cornell, U. Schwertmann, The iron oxides: structure, properties, reactions, occurrences, and uses, 2nd, completely rev. and extended ed., Wiley-VCH, Weinheim, 2003.**

2. **G. Cao, Nanostructures & nanomaterials: synthesis, properties & applications, Imperial College Press, London, 2004.**

3. **Q.A. Pankhurst, J. Connolly, S.K. Jones, J. Dobson, Applications of magnetic nanoparticles in biomedicine, J Phys D Appl Phys, 36 (2003) R167-R181.**

4. **S. Dutz, R. Hergt, Magnetic particle hyperthermia-a promising tumour therapy?, Nanotechnology, 25 (2014).**

5. **P. de la Presa, Y. Luengo, V. Velasco, M.P. Morales, M. Iglesias, S. Veintemillas-Verdaguer, P. Crespo, A. Hernando, Particle Interactions in Liquid Magnetic Colloids by Zero Field Cooled Measurements: Effects on Heating Efficiency, J Phys Chem C, 119 (2015) 11022-11030.**

Vedoucí bakalářské práce: **MSc. Ilona Smolkova, PhD.**
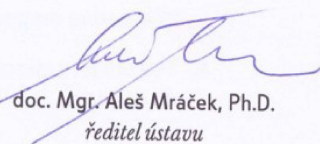Centrum polymerních systémů

Datum zadání bakalářské práce: **3. února 2017**

Termín odevzdání bakalářské práce: **19. května 2017**

Ve Zlíně dne 10. února 2017

doc. Ing. František Buňka, Ph.D.
děkan

L.S.

doc. Mgr. Aleš Mráček, Ph.D.
ředitel ústavu

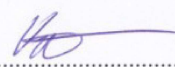Příjmení a jméno: Vítková Lenka   Obor: Materiálové inženýrství

PROHLÁŠENÍ

Prohlašuji, že

- beru na vědomí, že odevzdáním diplomové/bakalářské práce souhlasím se zveřejněním své práce podle zákona č. 111/1998 Sb. o vysokých školách a o změně a doplnění dalších zákonů (zákon o vysokých školách), ve znění pozdějších právních předpisů, bez ohledu na výsledek obhajoby [1];
- beru na vědomí, že diplomová/bakalářská práce bude uložena v elektronické podobě v univerzitním informačním systému dostupná k nahlédnutí, že jeden výtisk diplomové/bakalářské práce bude uložen na příslušném ústavu Fakulty technologické UTB ve Zlíně a jeden výtisk bude uložen u vedoucího práce;
- byl/a jsem seznámen/a s tím, že na moji diplomovou/bakalářskou práci se plně vztahuje zákon č. 121/2000 Sb. o právu autorském, o právech souvisejících s právem autorským a o změně některých zákonů (autorský zákon) ve znění pozdějších právních předpisů, zejm. § 35 odst. 3 [2];
- beru na vědomí, že podle § 60 [3] odst. 1 autorského zákona má UTB ve Zlíně právo na uzavření licenční smlouvy o užití školního díla v rozsahu § 12 odst. 4 autorského zákona;
- beru na vědomí, že podle § 60 [3] odst. 2 a 3 mohu užít své dílo – diplomovou/bakalářskou práci nebo poskytnout licenci k jejímu využití jen s předchozím písemným souhlasem Univerzity Tomáše Bati ve Zlíně, která je oprávněna v takovém případě ode mne požadovat přiměřený příspěvek na úhradu nákladů, které byly Univerzitou Tomáše Bati ve Zlíně na vytvoření díla vynaloženy (až do jejich skutečné výše);
- beru na vědomí, že pokud bylo k vypracování diplomové/bakalářské práce využito softwaru poskytnutého Univerzitou Tomáše Bati ve Zlíně nebo jinými subjekty pouze ke studijním a výzkumným účelům (tedy pouze k nekomerčnímu využití), nelze výsledky diplomové/bakalářské práce využít ke komerčním účelům;
- beru na vědomí, že pokud je výstupem diplomové/bakalářské práce jakýkoliv softwarový produkt, považují se za součást práce rovněž i zdrojové kódy, popř. soubory, ze kterých se projekt skládá. Neodevzdání této součásti může být důvodem k neobhájení práce.

Ve Zlíně 15. 5. 2014 ....

[1] zákon č. 111/1998 Sb. o vysokých školách a o změně a doplnění dalších zákonů (zákon o vysokých školách), ve znění pozdějších právních předpisů, § 47 Zveřejňování závěrečných prací:
(1) Vysoká škola nevýdělečně zveřejňuje disertační, diplomové, bakalářské a rigorózní práce, u kterých proběhla obhajoba, včetně posudků oponentů a výsledku obhajoby prostřednictvím databáze kvalifikačních prací, kterou spravuje. Způsob zveřejnění stanoví vnitřní předpis vysoké školy.
(2) Disertační, diplomové, bakalářské a rigorózní práce odevzdané uchazečem k obhajobě musí být též nejméně pět pracovních dnů před konáním obhajoby zveřejněny k nahlížení veřejnosti v místě určeném vnitřním předpisem vysoké školy nebo není-li tak určeno, v místě

pracoviště vysoké školy, kde se má konat obhajoba práce. Každý si může ze zveřejněné práce pořizovat na své náklady výpisy, opisy nebo rozmnoženiny.

(3) Platí, že odevzdáním práce autor souhlasí se zveřejněním své práce podle tohoto zákona, bez ohledu na výsledek obhajoby.

[2] zákon č. 121/2000 Sb. o právu autorském, o právech souvisejících s právem autorským a o změně některých zákonů (autorský zákon) ve znění pozdějších právních předpisů, § 35 odst. 3:

(3) Do práva autorského také nezasahuje škola nebo školské či vzdělávací zařízení, užije-li nikoli za účelem přímého nebo nepřímého hospodářského nebo obchodního prospěchu k výuce nebo k vlastní potřebě dílo vytvořené žákem nebo studentem ke splnění školních nebo studijních povinností vyplývajících z jeho právního vztahu ke škole nebo školskému či vzdělávacího zařízení (školní dílo).

[3] zákon č. 121/2000 Sb. o právu autorském, o právech souvisejících s právem autorským a o změně některých zákonů (autorský zákon) ve znění pozdějších právních předpisů, § 60 Školní dílo:

(1) Škola nebo školské či vzdělávací zařízení mají za obvyklých podmínek právo na uzavření licenční smlouvy o užití školního díla (§ 35 odst. 3). Odpírá-li autor takového díla udělit svolení bez vážného důvodu, mohou se tyto osoby domáhat nahrazení chybějícího projevu jeho vůle u soudu. Ustanovení § 35 odst. 3 zůstává nedotčeno.

(2) Není-li sjednáno jinak, může autor školního díla své dílo užít či poskytnout jinému licenci, není-li to v rozporu s oprávněnými zájmy školy nebo školského či vzdělávacího zařízení.

(3) Škola nebo školské či vzdělávací zařízení jsou oprávněny požadovat, aby jim autor školního díla z výdělku jím dosaženého v souvislosti s užitím díla či poskytnutím licence podle odstavce 2 přiměřeně přispěl na úhradu nákladů, které na vytvoření díla vynaložily, a to podle okolností až do jejich skutečné výše; přitom se přihlédne k výši výdělku dosaženého školou nebo školským či vzdělávacím zařízením z užití školního díla podle odstavce 1.

ABSTRAKT

Tato bakalářská práce je zaměřena na vícejaderné magnetické částice, jejich fyzikální a chemické vlastnosti, syntézu a aplikace, zvláště na léčbu nádorových onemocnění pomocí magnetické hypertermie. Nedávno bylo ukázáno, že vícejaderné magnetické částice mohou být efektivnější než jednotlivé nanočástice z hlediska generování tepla pod vlivem externího střídavého magnetického pole, a takto zvýšit léčebný efekt hypertermie. Nicméně, mechanismus generování tepla v takových materiálech není ještě zcela jasný. Experimentální část této práce se právě proto zaměřuje na stanovení souvislosti mezi magneto-strukturálními vlastnostmi vícejaderných magnetických částic a jejich chováním pod vlivem externího střídavého magnetického pole.

Klíčová slova: oxid železa, vícejaderné částice, magnetická interakce, magnetický koloid, měrná ztrátová energie, nanomagnetismus, hypertermie

ABSTRACT

This bachelor's thesis is devoted to multicore magnetic particles, their physical and chemical properties, synthesis and applications with a special focus on magnetic hyperthermia tumor treatment. Recently it was demonstrated that multicore magnetic particles could be superior over single nanoparticles in heat generation under exposure to an external alternating magnetic field, and thus could enhance the therapeutic effect of hyperthermia. However, the mechanism of heat generation in such materials is not clear yet. The experimental part of the current thesis focuses on the establishment of the correlation between magneto-structural properties of the multicore magnetic particles and their performance under exposure to an external alternating magnetic field.

Keywords: iron oxide, multicore particles, magnetic interaction, magnetic colloid, specific loss power, nanomagnetism, hyperthermia.

ACKNOWLEDGEMENTS

I hereby declare that I have worked out my Bachelor's thesis independently and on the basis of literature and sources listed in the Bibliography.

I hereby declare that the print version of my Bachelor's thesis and the electronic version of my thesis deposited in the IS/STAG system are identical.

CONTENTS

INTRODUCTION

The aggregates of magnetic nanoparticles (NPs), the so-called magnetic multicore particles (MCPs) are promising materials for application in medicine, as targeted drug delivery agents, magnetic resonance imaging (MRI) contrast agents, or magnetic hyperthermia mediators. The choice of materials for investigation was made with respect to the possibility of biomedical applications, therefore as the structural material of the primary NPs, magnetic iron oxides were used. Aside from being biocompatible, they show high magnetic performance and chemical stability. Citric acid and Al_2O_3 were used as modification agents due to their biocompatibility and good affinity to iron oxide. Water was chosen as a carrier liquid.

Theoretical part of the thesis provides a brief introduction to magnetism with special focus on magnetism at nanoscale. After that, magnetic iron oxides, being the main investigated objects in the thesis, are characterized from both physical and chemical point of view. Differences of magnetic iron oxide NPs from the bulk magnetite or maghemite are discussed. Their dispersion stability is also described and the options for stability enhancement are given. Synthesis procedures and methods of characterization are briefly introduced and possible applications are given with special focus on magnetic hyperthermia. The theoretical part is followed by the establishment of the aim of the work.

The goal of the current thesis is to establish the correlation between magneto-structural parameters of MCPs and magnetization dynamics in an alternating magnetic field (AMF). The properties of MCPs depend on the morphology of cores (i.e. primary NPs), type of magnetic interaction between them, on the size of MCPs and interaction between them, etc. In order to study the influence of cores morphology, samples of three different morphologies were prepared. Influence of MCPs size is studied via preparing dispersions of MCPs of different hydrodynamic size. Surface modified MCPs are made so as to enhance dispersion stability and to study the influence of magnetic interparticle interaction on their behavior in AMF.

Experimental part includes description of synthesis procedure of iron oxide primary NPs with three different morphologies, followed by creating stable dispersions of MCPs on the base of these primary NPs. The surface modification of MCPs leading to the increase of the long-term stability of the dispersions is described as well. The measurements to characterize magnetostatic and structural properties are specified in this part. Results of the measurements are given and discussed with respect to findings of previous studies made on this issue.

I. THEORETICAL PART

1 MAGNETISM

The theoretical part of the current bachelor's thesis will begin with the basic laws and phenomena of magnetism, that will be followed by the specific phenomena that occur at the nanoscale.

1.1 Basis of magnetism

To describe a magnetic field, following characteristics are used. Vector of magnetic field (*H*) is defined with respect to existence of electromagnetic field, and for a loop with a current it is:

$$\vec{H} = \frac{I}{2r} \ (1),$$

where *I* is the current and *r* is the radius of the loop. It is closely related to the vector of magnetic induction, so these two characteristics are often used to define each other. For magnetic induction the relation is:

$$\vec{B} = \mu_0 \vec{H} + \vec{J} \ (2),$$

where μ_0 is a constant called vacuum permeability and *J* is the vector of magnetic polarization. Magnetic polarization vector is defined as:

$$\vec{J} = \mu_0 \vec{M} \ (3).$$

In this relation *M* states for the vector of magnetization. Magnetization vector has its roots in the fact that a magnet contains many seperate magnetic moments, and the definition relation is:

$$\vec{M} = \lim_{v \to 0} \frac{\sum V \vec{p_M}}{v} \ (4),$$

i.e. sum of magnetic moments per volume unit.

Magnetic field vector can be defined using magnetic induction in this way:

$$\vec{H} = \frac{\vec{B}}{\mu_0} - \vec{M} \ (5).$$

As the basic characteristics of magnetic field are vectors, it is reasonable to expect the behavior of an object in a magnetic field to be strongly dependent on the direction of the field [1,2].

When speaking about magnetic field, electric field cannot be overlooked. The relation between these two phenomena is so close, that in many cases they are not distinguished at all and one speaks about electomagnetism. The relation is defined by Maxwell equations:

$$\nabla \times \vec{E} = \frac{-\partial \vec{B}}{\partial t} \ (6),$$

$$\nabla \cdot \vec{D} = \rho \ (7),$$

$$\nabla \times \vec{H} = \vec{j} + \frac{\partial \vec{D}}{\partial t} \ (8),$$

$$\nabla \cdot \vec{B} = 0 \ (9),$$

where E is the electric field vector, t is time, ρ is free electric charge density, j is conducting electric current density, D is electric displacement vector and is defined by relative permeability of the material (ε) and permeability of vacuum (ε_0) as:

$$\vec{D} = \epsilon \, \epsilon_0 \vec{E} \ (10),$$

A charged particle moving in a magnetic field could be described by the Lorentz force law, according to which the particle is affected by a force of:

$$\vec{f} = q \vec{v} \times \vec{B} \ (11),$$

where q is the charge of the particle, v is the vector of velocity and B is the vector of magnetic induction [1].

The energy of a magnetic material is given by magnetic exchange energy, domain wall energy and anisotropy energy. Magnetic exchange energy is described as the strength of coupling between ionic magnetic moments and is strongly temperature dependent [3]. The other energy participations will be discussed deeper in the next sections.

1.1.1 Magnetic ordering

Depending on the cooperation between atomic magnetic moments, we distinguish two types of magnetism: noncooperative and cooperative [4].

1.1.1.1 *Noncooperative magnetism*

Noncooperative magnetism can be further divided into paramagnetism and diamagnetism. Paramagnetism occurs in such materials, where identical, uncoupled atomic magnetic moments are located in isotropic surroundings. This allows the magnetic moments to partially align in an external magnetic field, though they lack long-range ordering. Diamagnetism, on the other hand, arises from the effect of an external magnetic field on an atomic inner electrons motion. Substances which are classified as diamagnetic have all the electrons coupled. Their shells are either full, or the valence electrons are coupled in molecular orbitals. Therefore the magnetization of such substance is negative. This phenomenon occurs in all substances, but is very weak, so it can be masked completely by presence of large paramagnetism [2,4].

1.1.1.2   Cooperative magnetism

Cooperative magnetism is actualized via exchange interactions between magnetic moments, either direct or indirect. Direct exchange occurs when moments are close enough to have overlap of their wave functions. Indirect exchange can appear between moments coupled over relatively large distances. If the indirect exchange is moderated by a nonmagnetic ion, it is called super exchange. This case is typical for magnetic iron oxides. These exchange mechanisms can result in two major arrangements: parallel alignment of magnetic moments, or antiparallel alignment. Substances with parallel alignment are called ferromagnetic. Substances with antiparallel alignment can be either ferrimagnetic, if the magnetic moments do not compensate, or antiferromagnetic, if the magnetic moments compensate. These states last until so-called Curie temperatures, where the thermal energy overcomes the exchange energy [4].

1.1.2   Magnetization hysteresis

To magnetize a ferromagnetic material, a work is required to be done by the applied magnetic field. The work is equal to the area enclosed by initial magnetization curve and ordinary axis. This energy is partially dissipated inside the material in the form of heat and partially stored. The magnetization cannot grow infinitely, but it reaches a maximum, called saturation magnetization, when all the magnetic moments within the crystal are aligned (Fig. 1). While demagnetizing, the magnetization does not follow the same curve, but creates a closed hysteresis loop. According to the area of this loop we divide magnetic materials into hard and soft magnets. Hard magnets have wide hysteresis loop. Therefore, they also have high remanence, high coercivity and large hysteresis losses. On the other hand, soft magnets have narrow hysteresis loop, which affects their behavior as follows: high permeability, low coercive force and small hysteresis losses [1].
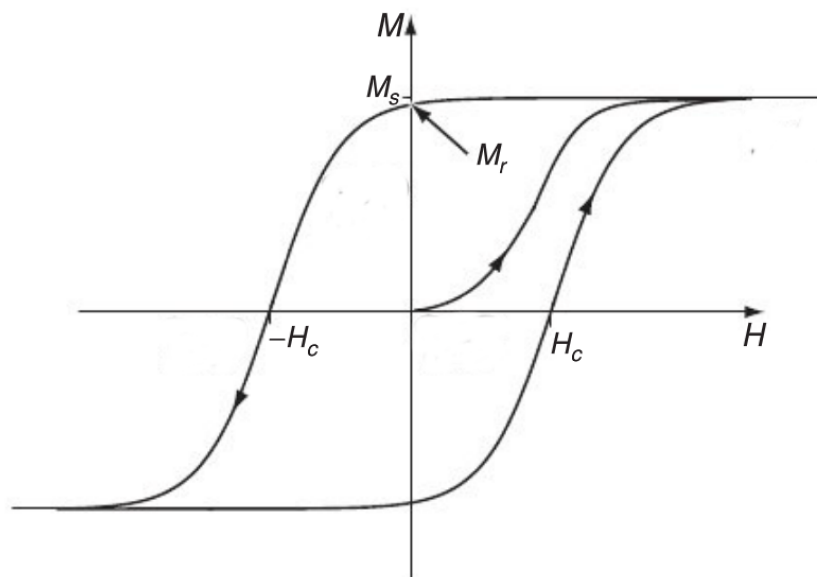
Fig.1: Initial magnetization curve and hysteresis loop, adapted from [5]; M_s stands for magnetization saturation, M_r magnetization remanence, H_C coercivity.

1.1.3 Magnetic anisotropy

As stated earlier, magnetization and other magnetic field characteristics depend strongly on the field direction. That means there is a preferred direction of the magnetization, and it is along the so-called easy axis. But this axis differs throughout the crystal and bulk material. In combination with demagnetizing forces at the grain borders, this leads to decrease of overall magnetization compared to saturation magnetization [2].

There are several types of anisotropy in magnetic materials. The overall free energy is determined by their combination. Three of them will be briefly introduced. Most of the others are highly dependent on the chemical structure of the material and therefore are not within the scope of the thesis.

1.1.3.1 Magnetocrystalline anisotropy

Magnetocrystalline anisotropy arises from the direction of magnetization within the crystal lattice. It can be quantified by energy necessary to flip the magnetization vector from easy axis to hard axis. It is explained by interaction of magnetic polarization moments, but this contribution is neglected unless there are no other causes of magnetocrystalline anisotropy. Greater contribution is given by crystalline electric field, exchange and spin-order interaction affected by **3d** or **4f** electrons. Magnetocrystalline anisotropy is grain size and shape independent [2,6].

1.1.3.2   Shape anisotropy

Magnetic moments of the atoms give arise to a so-called demagnetizing field within the grain or crystal. This field vector is generally non-uniform, even if the magnetic moments are aligned. It depends mostly on the shape of the crystal and consequently leads to shape anisotropy. For grains or particles with no shape anisotropy (spherical) it depends solely on the saturation magnetization, but when shape anisotropy occurs, the demagnetization becomes highly oriented and can partially determine the easy axis of the grain. The shape anisotropy energy can also be understood as the difference between the energies of the longest and shortest dimension of the grain. This type of magnetic anisotropy is negligable for bulk materials, where magnetocrystalline anisotropy is dominant. Shape anisotropy rises with decline of the size and growth of the saturation magnetization [2,6].

1.1.3.3   Magnetostriction

While magnetic material undergoes magnetization, it changes its dimensions. This affects the balance of forces within the crystal, like crystalline electric field interactions or pseudo-magnetic moments interactions, which leads to changes in magnetization. This phenomena is called magnetostriction. Introducing suffient stress along one axis can have the same effect. Therefore the magnetostriction is sometimes reffered to as stress anisotropy [2,6].

1.2   Macroscopic magnetism

The fact that a ferro- or ferrimagnet is not magnetized to saturation all the time is being explained by the domain theory. The basic principles of the domain structure and some of its conclusions will be discussed in this section.

In an infinite long magnet, the atomic magnetic moments would have aligned parallel to the long axis, creating two poles. Likewise in a finite sized magnet the magnetic moments align along the easy axis and create surface free poles. This leads to rise of magnetostatic energy and cosequently increase of exchange energy, magnetocrystalline energy or magnetoelastic energy. In other words, a demagnetizing field arises [1].

In order to minimize the energy of the system, the magnetic moments align parallel or antiparallel to each other. The most advantageous arrangement appears to be the domain structure. A domain is an area within the magnet with parallel alignment of magnetic moments. The domains are oriented in a way that creates a closed loop of magnetic flux. The direction of the moments changes at the domain walls, which are energetically richer than the inside of a domain. There are two possibilities

for the domain wall. Either the direction changes gradually, or abruptly. In the first case, exchange energy is minimized due to small angles between the moment vectors. On the other hand, anisotropy energy is high due to deviations from the easy axis direction. In second case it is the opposite way. It is clear that energy is stored inside the domain walls and in order to create parallel alignment throughout the whole structure, i.e. reach saturation magnetization, it must be overcame [1,5,7].

1.3 Nanoscale magnetism

If a static magnetic field exists in finite space, another potential energy, the Zeeman energy, must be taken into account. It is equal to work required for a magnetic moment to be brought from infinity to a place of magnetic potential p_J within the magnetic field. It is also the energetic change of the system after such action [6].

For any given magnetic material, there is a grain size below which it no longer contains domain walls, therefore all the magnetic moments are aligned. This phenomenon is called the single-domain (SD) state. In contrast to multi-domain (MD) systems, the energy required to rotate the magnetization in SD particle is much higher than for changing the magnetization via transition of domain walls. The SD-MD transition size varies depending on magnetization saturation and grain shape. With decrease of magnetization saturation, the transition size increases [2].

According to Stoner-Wohlfarth model, total energy of a single domain NP is given by both anisotropy energy and Zeeman energy [3]. It leads to equation:

$$E_{tot} = KV\sin^2\Theta - \vec{H}VM_s\cos(\Theta - \varphi) \quad (12),$$

where, K is the uniaxial magnetic anisotropy, H is the applied field, V is the NP volume, M_s is the saturation magnetization, θ is the angle between the easy axis and the NP magnetization, and ϕ is the angle between the easy axis and the applied magnetic field [3].

1.3.1 Superparamagnetism

SD particles can reach another turning point, when their remanence and coercivity declines to zero (Fig. 2). This state resembles the paramagnetic state, but has different relaxation times. That is why it is called the superparamagnetic (SPM) state. This phenomenon is caused by thermal energy prevailing the anisotropy energy, which allows the magnetization to rotate freely, thus demagnetizing the particle. The relaxation time for SPM particles is derived as follows:

$$\frac{1}{\tau} = f_0 \frac{e^{-K_u V}}{kT} \quad (13),$$

where τ is the relaxation time, f_0 is the frequency factor, K_u is the anisotropy constant, V is the particle volume, k is the Boltzmann constant and T is the thermodynamic temperature. As evident, the SPM behavior is dependent on particle volume and temperature. For any given magnetic material there is a critical size (D_{sp}) at which superparamagnetism appears. With respect to the speed of change in magnetic field (let it be labeled t) it is possible to define blocking temperature or blocking volume, at which $\tau \gg t$. This results in magnetization transitioning from unstable state to a stable one. Experiments have shown that the same effect can be reached by high-frequency AMF, therefore a blocking frequency can be defined as well. Above this frequency the so-called dynamic hysteresis arises and the energy is eliminated into heat, which is used in magnetic hyperthermia that will be discussed later [2,3,8].
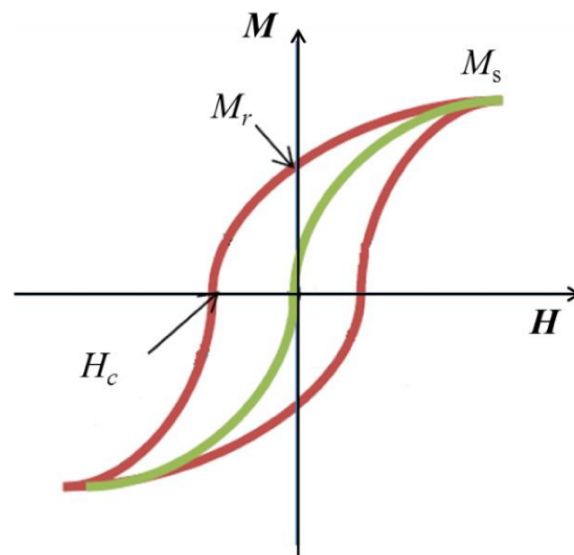

Fig.2: Magnetization curves of SD (red line) and SPM (green line) NPs, source [8].

2 MAGNETIC IRON OXIDES

This thesis aims on magnetic iron oxides, namely magnetite and maghemite, and their possible applications in medicine. In this section, structure and basic physical and chemical properties of bulk magnetite and maghemite will be discussed.

2.1 Physical properties

At first it is necessary to introduce the crystalography of iron oxides in order to better understand their magnetic behavior.

2.1.1 Crystal structure

Magnetite (Fe_3O_4) has a unique structure among iron oxides due to consisting of both Fe^{II} and Fe^{III} ions. Its unit cell is face-centered cubic with an edge lenght of a = 0,839 nm. The presence of both divalent and trivalent iron ions causes the layers to be compound of either octahedral or mixed tetrahedral and octahedral structure units. As these layers stack, they form inverse spinel structure. In case when the octahedral sites are ordered, the spinel is undefected. Stoichiometric magnetite has the molar ratio of Fe^{II}/Fe^{III} = 0,5. In non-stoichiometric magnetite, an Fe^{2+} cation deficient sublattice emerges [9].

Maghemite (γ-Fe_2O_3) is very similar to magnetite in terms of structure, but all or most iron ions are in trivalent state. Instead of Fe^{II} ions vacancies occur. The unit cell of maghemite is cubic with an edge lenght of a = 0,834 nm. Synthetic maghemite often displays so-called vacancy ordering structure. This happens due to the preparation methods being based on oxidizing of magnetite. As the vacancies cannot order in cubic cell unit due to their fractional number, the unit cell changes from cubic to tetragonal [9].

2.1.2 Magnetic properties

In bulk magnetite or maghemite, the magnetic interaction happens mostly via electrostatic exchange interaction. It causes the material to display ferrimagnetic behaviour. The magnetization is so strong that magnetite was for long considered to be a ferromagnet, until Néel explained the interaction mechanism. The exchange mechanism is in particular the so-called super exchange, mediated by O^{2-} or OH^- ions. In magnetite, delocalized electron system can occur due to co-presence of Fe^{2+} and Fe^{3+} ions [2,9].

At the atomic level, magnetic behaviour of magnetite and maghemite arises mainly from polarization of **s** electrons by **3d** electrons present in the outer shell. Less significant part of the

magnetization is provided by polarization of **s** electrons by surrounding cations and also by spin dipole of **3d** electrons own to the atom [9].

If maghemite keeps the vacancy ordering (see above), and therefore the inverse spinel structure, vacancies naturally appear in magnetic structure as well. Although this vacancies are in octahedral sites, the magnetic moment is still greater than on the tetrahedral sites due to the excess of Fe^{3+} ions [7].

2.2 Chemical properties

Iron oxides consist of iron and oxygen atoms in various ratios. Iron is found in two oxidational states - as Fe^{II} and Fe^{III}. Its best known oxides are FeO, α-Fe_2O_3, γ-Fe_2O_3 and Fe_3O_4. Fe^{II} is less stable than Fe^{III}, therefore FeO, γ-Fe_2O_3 and Fe_3O_4 transform themselves into one another either spontaneously, or under specific conditions, such as elevated temperature. Transformation into α-Fe_2O_3 is more difficult due to different crystal structure [10].

As mentioned above, typical feature of magnetite is the co-existence of Fe^{2+} and Fe^{3+} ions inside the crystal structure. Fe^{2+} ions are unstable and undergo oxidation to Fe^{3+} easily. This process can be slowed down by decreasing temperature, or stopped by eliminating oxygen from the environ [9].

2.2.1 Oxidation of magnetite

When left in an air atmosphere, magnetite oxidizes into maghemite rather rapidly. This process is accompanied by morphological changes within the crystal structure, and therefore changes of certain physical properties as well. Oxidation occurs also in water, alkaline and acidic media. The hydrothermal oxidation is reported to be slower than the air oxidation, but the main principal that will be explained in the next paragraph, remains the same [9].

At first, several Fe^{2+} ions oxidize and the Fe^{2+}/ Fe^{3+} ratio decreases. Then Fe^{3+} ions migrate via diffusion towards the surface leaving vacancies and creating a layer of maghemite. As the oxidation proceeds, the density of material decreases. In completely oxidized magnetite, i.e. maghemite, the cubic unit cell edge lengh is smaller (see above). That means the morphology of crystals changes throughout the oxidation process [9].

As the transformation occurs via diffusion, it is clear that the process is much more rapid in small crystals than in large crystals due to different path lengths. It has also been found that in natural crystals the oxidation proceeds more slowly and sometimes does not terminate at all. This is being explained by the absence of OH^- in natural magnetite, which is therefore considered to serve as a prerequisite for the transformation [9].

3 MAGNETIC IRON OXIDE NANOPARTICLES

Phenomenological behavior of NPs depends on many aspects, such as particle size, shape, or the environs of the particle. Aside from this, some of the interface effects will be discussed in this section.

3.1 Physical properties

Basic physical properties are strongly size-dependent at nanoscale. For ultrasmall NPs quantum behavior arises and fades away when dimensions of bulk material are reached. Between these two extremes, the behavior tends to be non-linear and material specific [11].

3.1.1 Magnetic properties

Magnetic properties of NPs, as well as many other physical properties, are strongly size-dependent. For magnetite, critical size of SD transition (see above) is approximately 20 nm, whereas for iron oxides with lower saturation magnetization, such as hematite, the critical size can reach up to 15 μm. Critical SPM size value lies around 13 nm. The magnetic behavior is also influenced by the NPs magnetic interactions, leading to the formation of clusters or MCPs consisting of SD cores [2,8].

3.2 Structural properties

Crystalography of magnetite and maghemite remains the same in bulk material and in the NPs. But the finity of NPs, alongside with great surface to volume ratio, gives them some unique properties.

Due to thermodynamic instability of the system, magnetic NPs undergo aggregation very easily. As this field of study is rather new, the terminology is not clear yet. The assemblies are called multicore particles, or nanoclusters. The term multicore particle can be used for closely packed NPs where magnetic exchange can occur, whereas nanocluster is used for rather loose assemblies with weak magnetic coupling. However, in many cases these terms are being counterchanged [3,12–14], so in this thesis, the term MCPs will be used for packed aggregates of NPs and the term nanocluster will not be further used.

In contrast to single-core particles, MCPs magnetization depends on the individual magnetic moments of the cores (i.e. crystals) as well as on the effective magnetic moment (Fig.3), which is the vector sum of the magnetic moments of the cores. Their behavior in an AMF magnetic field, especially Néel and Brown relaxation, are determined by magnetic interactions among the cores, size distribution of crystals and magnetic anisotropy (see above). Aside from Brown or Néel

relaxation dominance, a distinct difference in the magnetization curve exists. Magnetization of single-core particles increases more rapidly with increasing magnetic field than it does for multicore ones. It can be explained by slower aligning of the effective magnetic moment of an MCP with the field, which cannot happen for single-core NPs. With respect to AMF frequency, the multicore behavior can be suppressed and at high frequencies the single-core behavior is very strong [14].
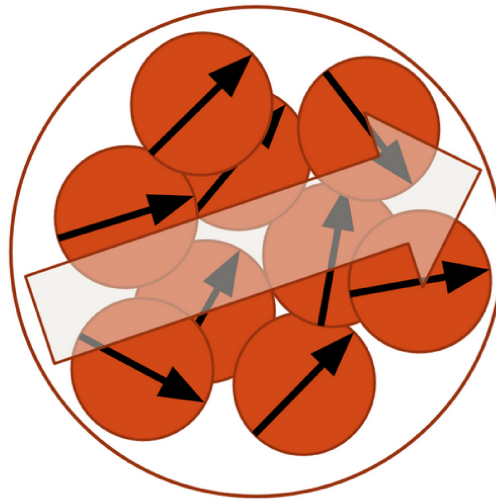
Fig.3: Scheme of an effective magnetic moment within an MCP.

3.3 Colloid dispersion

A colloid system is typically defined as a system, where dispersed phase falls in size range from 1 nm to 1 µm. Their unique characteristics come mainly from the fact that many physical phenomena and chemical reactions take place at the interface. As the diameter declines, the specific surface, i.e. the fraction of molecules located at the interface, grows. The colloid dispersions in general, including those of magnetic iron oxides, are thermodynamically unstable systems. In order to prevent aggregation and coagulation from the solution, certain precautions must be taken [15].

3.3.1 Methods of stabilization

The colloid dispersion remains in metastable state as long as its energy is lower than the energy barrier, which is given by repulsive forces between the colloidal particles. The coagulation process happens due to collisions of particles of sufficient energy. The colloidal particles, due to Brown motion, move with the translational energy of:

$$E_k = \frac{3}{2} k T \quad (14),$$

where k stands for Boltzman constant and T for thermodynamic temperature. Most of the stabilization methods focus on increasing the energy barrier, therefore lowering the probability of

coagulation. Another option is decresing the temperature, which leads to decrease of translational energy [15].

3.3.1.1 Electrostatic repulsion stabilization

Electrostatic repulsion stabilization methods are based on the existence of electric double layer at the surface of charged particles. The inner layer is either a part of the particle, or it is made of a single ion adsorbed layer. The outer layer is best described by Stern model, which presumes both electrostatic and adsorption forces having an effect on the outer ions. As the radius increses, the adsorption forces decline more rapidly than electrostatic forces. The point where adsorption forces fade away is called the Stern layer. As the layer is of the same sign at each particle, it induces repulsive force if the particles get close enough. At the same time, ever-present van der Waals attractive forces push the particles closer together. For magnetic NPs magnetic interactions also contribute to the overall system energy. The total interaction energy is:

$$\Delta G_{tot} = -\Delta G_{at} + \Delta G_{rep} \quad (15).$$

As evident from eq. 15, it depends on the energy of attractive (G_{at}) and repulsive (G_{rep}) forces, respectively. If ΔG_{tot} reaches zero, the system undergoes rapid coagulation. The electrostatic forces arising from the double layer are characterized by Stern potential, or zeta potential, which responds to the energy needed to move a ion onto the Stern layer. The zeta potential depends strongly on the concentration of electrolyte. With increase of the concentration, the electrostatic repulsion declines and coagulation becomes more probable. Magnetite NPs could be electrostatically stabilized by charging their surface by acids or alcalis [15,16].

3.3.1.2 Steric stabilization

Steric stabilization is based on a lyophilic colloid adsorbing to the particle surface and creating a compact layer. When two coated particles approach each other, the layers interpenetrate. This leads to osmotic effect and volume restriction effect. Both of these effects result in entropy decrease, which is thermodynamically unfavorable and the system regains the entropy by moving the particles apart. Polymers are often used as steric stabilizers because their long chains provide very good steric stabilization effect. Stabilization of magnetite NPs with poly(acrylic acid) is a typical example. The carboxylic groups of poly(acrylic acid) are chemically adsorbed to the charged surface of magnetite and the alkyl chains provide steric barrier. The steric stabilizers do not need to be charged, but electrostatic and steric stabilization can be combined [15,17].

3.3.1.3 Nanoparticles haloing

A novel approach to stabilize weakly charged colloids has been studied recently. It uses highly charged colloid NPs in mixture with weakly charged ones. For example, Zubir et al., 2015 [18] studied weakly charged TiO_2 and Fe_3O_4 NPs mixed with highly charged Al_2O_3 NPs at various ratios. The results confirmed higher stability of the dispersion at the isoelectric point of weakly charged particles and zeta potential close to the one of pure Al_2O_3 dispersion. TEM micrography suggests the following stabilization mechanism. The highly charged particles surround the weakly charged ones and create an electrostatic barrier. This method resambles the electrostatic repulsion stabilization, but unlike other methods uses no surfactant, as the NPs do not create chemical bond. As the nature of this phenomenon is electrostatical, it depends highly on pH of the media. Also the concentration factor is important, because a compact layer around the particle is needed for effective haloing [18,19].

3.4 Synthesis

The methods of iron oxide NPs synthesis can be divided into two major groups: top-down (physical) methods and bottom-up (chemical) methods. Examples of both approaches will be given in this section. Magnetite NPs can be also synthetized biochemically by magnetotactic bacteria.

3.4.1 Top-down methods

There is a confuse in terminology regarding the major top-down methods, as different authors use terms gas phase preparation and laser evaporation to describe different methods, and sometimes these terms are being counterchanged [11,13,20]. In this section, a summary of the basic characterizations common to all the methods will be provided.

The basic principle is evaporation of an iron containing material into gas phase by a powerful energy source, followed by condensation of NPs. There is a high variability of parametres allowing the NPs to be tailored according to their intended purpose. When carefully conducted, this procedure can give particles of narrow size distribution and high uniformity. The main influences on the particle structure are the nature of evaporated material, the carrier gas flux and the power of the energy source. The nature of the carrier gas is irrelevant in most cases, because it is innert to final products. As the source of iron, bulk magnetite or maghemite, magnetite powders of various grain size, or organometallic compounds can be used. The most common energy source is a laser, although other possibilities, such as microwave heating, have been studied due to rather low uniformity of the NPs provided by laser evaporation. After-synthesis treatments include mass spectroscopy separation, dispergating in water and surfactant coating. In contrast to bottom-up

methods, it is impossible to obtain single-core particles due to absence of opportunity to cover the cores with surfactant while growing [11,13,20].

3.4.2 Bottom-up methods

Coprecipitation of Fe^{II} and Fe^{III} salts in base media, also known as the Massart procedure, is a set of inorganic reactions involving hydrolysis, condensation and complexation. It can be conducted under mild conditions (non-toxic reagents, temperature below 100 ºC) and yields biocompatible iron oxides. However the size distribution is broad, therefore size selection follows the synthesis in order to increase reproducibility of the results for magneto-structural properties, which are often size-dependent. Surfactants of various nature are often used to prevent aggregation and/or increase colloid stability. If used during the very coprecipitation process, they can even ensure yielding of single-core NPs. Citric acid has been successfully used as a precursor to control the NPs size in the range or 5 - 15 nm [13]. Other possible surfactants include polyols or silica. The suitable surfactant is chosen with respect to anticipated purpose of the NPs and can be also an antibody, which is beneficial for example in targeted drug delivery application [8,12,13].

Polyols synthesis is essentially an oxidative hydrolysis of Fe^{2+} and Fe^{3+} salts in alkali in a stoichiometric mixture of polyols. This method allows a great variability in final NPs properties, due to an easy controlability of reaction conditions. The choice of used polyols, their ratio in the reaction mixture, the reaction temperature and duration influence the size and shape of the NPs obtained and can be altered very simply. The polyol solvents and precursors work also as surfactants, so the size distribution of the NPs is usually narrow. By choosing proper precursor, reagents ratio and other conditions, single-core particles can be obtained. As the synthesis is conducted under higher temperatures, the crystallinity is also very good, which leads to favorable magnetostatic properties [13,20].

Thermal decomposition of organometallic compounds is usually being conducted in two major ways - either the organometallic compound is injected into boiling surfactant solution, or it is boiled under controlled conditions. The cores obtained by this synthesis have nearly monodisperse size distribution and good crystallinity. As the surfactants are present during the synthesis, it is easy to prepare single-core particles using this method. A great disadvantage with respect to biomedical use is that mostly the NPs are hydrophobic. Therefore, careful removal of reaction mixture residues and replacement of the original surfactant is crucial. This brings up the problem of possibly irreversible aggregation while transfer into water solvent and this step needs to be done with particular caution [13,20].

3.5   Application

As the research of NPs continues, magnetic NPs find their way in technological applications like data storage, environmental protection, toxic inorganic and organic substances removal, or medicine, due to magnetite NPs biocompatibility and low toxicity [8,11,21].

3.5.1   Magnetic hyperthermia

The definition of hyperthermia, according to National Institute of Health, is a type of cancer treatment, in which body tissue is exposed to high temperatures to damage and to kill, and/or to make them more sensitive to the effects of radiation and cytotoxic drugs. This method is based on the fact that tumor tissues are generally more vulnerable to high temperatures. They become damaged at the temperatures around 41 ℃, while healthy tissues sustain undamaged up to 44 ℃ [8].

The elevated temperature can be induced by many techniques. In magnetic hyperthermia, an AMF is applied to cause heating of mediators. Mediators are magnetic materials placed inside a tumor. This way ensures the treatment to be local and minimizes the side effects of strong magnetic fields or long exposure of healthy tissues to high temperatures [8]

In order to maximize the heating effect, heating mechanism of magnetic NPs must be understood. There are three major heating mechanisms - eddy current heating, frictional heating and relaxation hysteresis losses. In 2002, Rosenweig proposed an explanation of heating mechanism by the linear response theory. This theory gives an expression for power dissipation:

$$P = \mu_0 \pi X^{''} f H^2 \ (16),$$

where, H and f are the amplitude and frequency of the AMF, respectively, μ_0 represents the permeability of free space, and χ'' is the out-of-phase component of the colloidal magnetic fluid AMF susceptibility. χ'' is determined by both Brown and Néel relaxation times. The Brown relaxation is related to NP's reaction to AMF by rotating as a whole. On the contrary, Néel relaxation represents the rotation of magnetic moment within the particle [3].

Current effort is to tailor the NPs in a way that enhances the relaxation hysteresis losses. Interestingly, even SPM NPs can produce heat by relaxation losses, when AMF of sufficient frequency, i.e. blocking frequency (see 1.3.1) is used. Studies have shown that not only size, but also shape are of great influence on heating efficiency [3,14]. Shape anisotropy usually increases the magnetization, and surface anisotropy seems to multiple the power dissipation in comparison to isotropic, i.e. spherical NPs. However, when the shape anisotropy is too high, it can cause the dynamic hysteresis (i.e. the hysteresis loop created by high-frequency AMF) to fade away.

Additionally, magnetic interactions among cores within an MCP, and mutual magnetic interaction of MCPs affect the heating as well [3,14].

Iron oxide NPs are being studied as promising candidates for magnetic hyperthermia treatment. The single-core SPM particles hold zero remanence magnetization and therefore do not tend to aggregate. Moreover, their small size (less than 20 nm) allows them to migrate freely through the blood vessels. However, their small relaxation losses cause them to have a very small heat outcome. This can be solved by MCPs, which, unlike single-core NPs, display hysteresis losses, yet no remanence magnetization. Such state is reffered to as superferrimagnetic [22].

3.5.2 MRI contrast agents

MRI is a diagnostic method based on magnetic resonance relaxation time of water in different types of tissue. This procedure is sensitive to complex state of the tissue, thus it gives much wider information about the patient [23].

MRI contrast aqgents improve the contrast image by alternating relaxation times of water surrounding the agent. The iron oxide NPs seem to be very promising in this matter, as they provide measurable effect at nanomolar concentrations. Other advantages are biocompatibility, ability to bond with antibodies, which enable the particles to be targetely delivered, possibility to combine MRI with magnetic hyperthermia and more [23].

3.5.3 Magnetic Particle Imaging

Magnetic Particle Imaging (MPI) is a progressive diagnostic method, which can be an alternative to MRI and in some applications beneficial in comparison. It uses SPM NPs as tracers and measures the magnetic field they generate. As the effectivity is mainly determined by Brown and Néel relaxation, the same process that has a great influence on magnetic hyperthermia effectivity, the main interest is to fabricate magnetic NPs suitable for combination of these two treatments with good results. Iron oxide NPs seem to be very promising in this field [3,23].

3.5.4 Data Storage

Although this thesis is meant to enlighten properties of magnetic NPs which are important for medical use, let us look over one possible technical application - data storage. As the computers become more sofisticated, the areal density of hard drives is increasing. Nowadays, this progress faces a problem with overheating. SPM NPs do not produce heat while demagnetizing, so they are very promising material for this use. However, there are still issues of stability and writability that need to be dealt with [11].

3.6 Methods of nanoparticles characterization

3.6.1 Laser Doppler Velocimetry

Laser Doppler Velocimetry (LDV) in combination with the electrophoretic experiment can be used to determine the zeta potential of charged particles (see 3.3.1.1). Electrophoresis is an electrokinetic effect induced by placing a charged particle in an electric field. The ions are attracted to the opposite charged pole of applied field. At the same time, viscous forces restrain this movement. Once the electrostatic and viscous forces reach equilibrium, the charged particles move with constant velocity, i.e. electrophoretic mobility. With the knowledge of the electrophoretic mobility it is possible to calculate the particle zeta potential using Henry equation:

$$U_E = \frac{2 \epsilon \zeta f(Ka)}{3 \eta} \quad (17),$$

where U_E is the electrophoretic mobility, ε is the dielectric constant of the particles, ξ is the zeta potential, $f(Ka)$ is the Henry's function and η is the viskozity of the media [24].

The measurement is conducted in the following way: an electric field is applied to the sample, i.e. electrophoretic effect is induced. Then the electrophoretic mobility is established using LDV. This technique uses coherent beam (i.e. a laser) to enlighten the sample and evaluates the fluctuations of scattered light risen from the Doppler effect. The fluctuations are proportional to the particle movement velocity and so they can be used to determine the electrophoretic mobility, since the electric field properties are known. For succesful measurement it is crutial to avoid any hydrodynamic or electroosmotic phenomena, which occur especially at the cell walls, and therefore construction of measuring device can be challenging [24].

3.6.2 Dynamic Light Scattering

Dynamic Light Scattering (DLS) is an analytical method designed for particle size measurement. The basic principle uses the Brownian motion velocity to calculate the particle size using Stokes-Einstein equation:

$$D = \frac{k_B T}{6 \pi \eta r} \quad (18),$$

in which D is the diffusion coeficient, k_B is the Boltzman constant, T is temperature, η is the viscosity of the media and r is the radius of the particle. From this equation it is clear that the diffusion coeficient is inversely proportional to the particle radius, so the smaller particles move faster through a fluid. As the calculation consideres the particles to be spherical, this technique

provides the hydrodynamic size, i.e. the size of a sphere which would move with the same velocity as the real particle does. It also represents the biggest dimension of the particle [25].

The measurement is conducted in the following way: (i) sample is enlighted by a coherent beam and the scattered light is written down with respect to the time; (ii) scattered light intensities fluctuations in time are measured, until such time when the correlation function drops to zero; (iii) from the duration of this time, the Brownian motion velocity is determined, and consequently used to calculate the hydrodynamic particle size, as was stated earlier. The DLS measurement is a fast and simple analysis method, but faces certain limitations. These are for example a necessity of very low sample concentration, or disregarding other interparticle forces, i.e. van der Waals or electrostatic forces, besides the ones responsible for Browninan motion [25].

3.6.3   Energy Dispersive X-ray Fluorescence Spectroscopy

Energy Dispersive X-ray Fluorescence Spectroscopy (ED-XRF) is one of the analytical methods known as X-ray spectroscopy. The basic principle of all these methods lies in the unique energy levels of the electrons (i.e. Pauli principle). High energy radiation, such as X-rays or γ-rays, is capable of causing an inner-shell electron to be ejected from the atom, leaving a hole in its place. The hole is consequently filled by an electron from a shell of higher energy. The difference in energy is balanced via radiating a photon. As stated earlier, this energy is element-specific due to Pauli principle. These so-called secondary photons are analysed in ED-XRF with respect to their energy diversity. Therefore, it is possible to analyze the sample both quantitatively and qualitatively [26,27].

3.6.4   Specific Loss Power Measurement

Heating efficiency of magnetic material in AMF is described by specific loss power (SLP), commonly measured with calorimetric method. High-frequency AMF is usually provided by a coil with alternating current. A thermoprobe is used to detect the temperature differential with dependence on time. The SLP can be easily calculated using following relation:

$$SLP = \frac{C_p}{m_{mag}} \cdot \frac{dT}{dt} \quad (19),$$

where C_p is the overall heat capacity of the sample, m_{mag} is the mass of magnetic material and dT/dt is the slope of the temperature rise curve. For the accuracy of this method, it is necessary to ensure adiabatic conditions. For that matter, adiabatic shields or vacuum are used [3].

3.6.5 Transmission Electron Microscopy

Transmission Electron Microscopy (TEM) is a microscopic method capable of high magnification (up to 10^6) as well as high resolution. This is given by the nature of illuminating beam, which for TEM consists of high-energy electrons. According to de Broglie relation, the wavelengths of such electrons are very short [27].

During TEM measurement, the sample is penetrated by the primary electron beam, which goes through either undeflected, or deflected. Two types of scattering processes can occur during the electron passage through the sample. Elastic scattering provides diffraction patterns and involves no energy losses. Inelastic scattering has origin in energy absorption and scattering at the heterogenities within the sample. This is the reason of spatial variation in the intensity of transmitted electrons [27].

Although TEM is a plentifully used method due to the great magnification or resolution, there are shortcomings to it. There are certain demands on the sample, such as low thickness, absence of fluids and ability to withstand the high-energy electrons beam unchanged. Also the depth resolution is limited and the TEM images are projected in 2D, despite the structures being 3D [27].

3.6.6 Vibrating Sample Magnetometry

Vibrating Sample Magnetometry (VSM) is a convenient method used for magnetic measurements on samples of small diameter, which cannot be tested in a closed magnetic circuit devices. This method uses the Faraday laws of electromagnetic induction to detect the magnetic moment of the sample. The measurement device consists of a strong electromagnet, a vibrating sample holder and four pickup coils surrounding the sample. The sample is magnetized by strong external magnetic field induced by the electromagnet and consequently induces voltage within the pickup coils when vibrating. This voltage is proportional to the vibration frequency and magnetic moment of the sample. VSM is capable of measuring wide range of magnetic properties, including hysteresis loop, via changing the magnetic field of the electromagnet, therefore changing magnetization of the sample. As the induced voltage is very small, a sensitive detector is needed. Reference magnets or capacity sensors are the most commonly used in VSM [28].

II. EXPERIMENTAL PART

4 AIM OF WORK

The aim of this thesis is to establish a correlation between magneto-structural properties of iron oxide MCPs and their heating efficiency in AMF. Heating efficiency in AMF was studied depending on the morphology of primary NPs, hydrodynamic size of MCPs and interparticle interactions between the MCPs. The intention was to give an insight into this phenomenon of MCPs, which has not been fully clarified yet, and to decribe a synthesis method which can be used to tailor the MCPs in a way which is the most suitable for application in magnetic hyperthermia treatment.

5   SAMPLE PREPARATION

In this section, magnetite NPs preparation by coprecipitation of iron salts and further modifications to obtain a stable colloid system will be introduced.

5.1   Chemicals

$FeCl_2 \cdot 4H_2O$ – puriss.p.a., $\geq$ 99%; $FeCl_3 \cdot 6H_2O$ – ACS reagent, 97%; HCl – ACS reagent, 37%; citric acid - ACS reagent, $\geq$99,5%; Al_2O_3 nanopowder - 13 nm primary particle size; agar were purchased from Sigma Aldrich; NH_3 – water solution 25-29% p.a. was purchased from Penta s.r.o.; Argon (Ar) was purchased from SIAD Czech s.r.o.

5.2   Magnetic iron oxide NPs synthesis

Before synthesis, argon was bubbled through demineralized water in order to oust oxygen. Solution of salts was prepared by dissolving 0,0125 mol of $FeCl_2 \cdot 4H_2O$ and 0,025 mol of $FeCl \cdot 6H_2O$ in 30 ml of water. 0,38 $mol \cdot dm^{-3}$ solution of ammonia was prepared by adding 29 ml of concentrated solution of ammonia (25 – 29 wt%) into a volumetric flask of 500 ml and filled up with water. The reaction was conducted at 70 °C under an innert atmosphere (Ar) and continuous stirring at 700 rotation per minute (rpm). The equipment for synthesis is depicted in Fig. 4.

By varying the reaction parameters three different samples of iron oxide NPs were obtained that were further used for preparation of water dispersions of MCPs.

In first case, 300 ml of the prepared ammonia solution was poured into a boiling flask. Then the solution of iron salts was slowly (6 – 8 drops per minute) added into the ammonia through a dropping flask. By this way, primary particles named sample 1 were obtained (see table 1).

In second case, the solution of salts was added abruptly (approximately 30 drops per minute) into 300 ml of ammonia solution. The primary particles prepared this way are named sample 2 (see table 1).

In third case, the solution of salts was poured into the boiling flask and 300 ml of ammonia solution was added dropwise (40-50 drops per minute). This procedure was used to obtain primary particles named sample 3 (see table 1). In all cases, the mixture was kept at 70 °C and stirred at 700 rpm for one hour after mixing of all the reagents.

Fig. 4: Assembly used for iron oxide NPs synthesis.

Table 1: Summary of symbols used for bare and surface modified samples

Primary NPs name	Primary particle morphology	Electrostatic stabilization of water dispersion, pH interval	Sample name	Modification agent	Sample name
Sample 1	Spherical, average particle size d=13 nm, polydispersity 0,3	1,5-2,5	S1_pH2	Citric acid	S1_pH2_cit.acid
				Al$_2$O$_3$ NPs	S1_pH2_Al$_2$O$_3$
		2,5-3,5	S1_pH3		S1_pH3_Al$_2$O$_3$
		3,5-4,5	S1_pH4		S1_pH4_Al$_2$O$_3$
		4,5-5,5	S1_pH5		
Sample 2	Spherical, d=13 nm, polydispersity 0,4	1,5-2,5	S2_pH2		
		2,5-3,5	S2_pH3		
		3,5-4,5	S2_pH4		
Sample 3	Variable in shape and particle size	1,5-2,5	S3_pH2		
		2,5-3,5	S3_pH3		

After the synthesis, NPs of all three samples sediment at the bottom of the flask (Fig. 5). NPs obtained represent aggregates with different hydrodynamic sizes. To separate aggregates of defined size (i.e. MCPs), peptization by acidification was performed.

Fig. 5: Sedimentation of MCPs at the bottom of the flask after synthesis.

5.3 Acidification and peptization

The NPs of the three samples were decanted and washed with water until neutral pH. In order to obtain stable dispersion of MCPs, the samples were treated with 0,001 mol·dm^{-3} HCl until pH of the mixture was 2 or lower. Several washes were needed. At this point peptization occurred either spontaniously, or after 20 min of ultrasonic treatment. After that water was gradually added in order to increase pH of the mixture. During this process, samples of supernatant were taken at several different pH values (Fig. 6). In order to increase concentration of NPs, the mixture was ultrasonicated for 15 min before collecting each sample. By this way, water dispersions of MCPs with certain hydrodynamic size based on primary NPs of samples 1, 2, or 3 were obtained (Table 1).
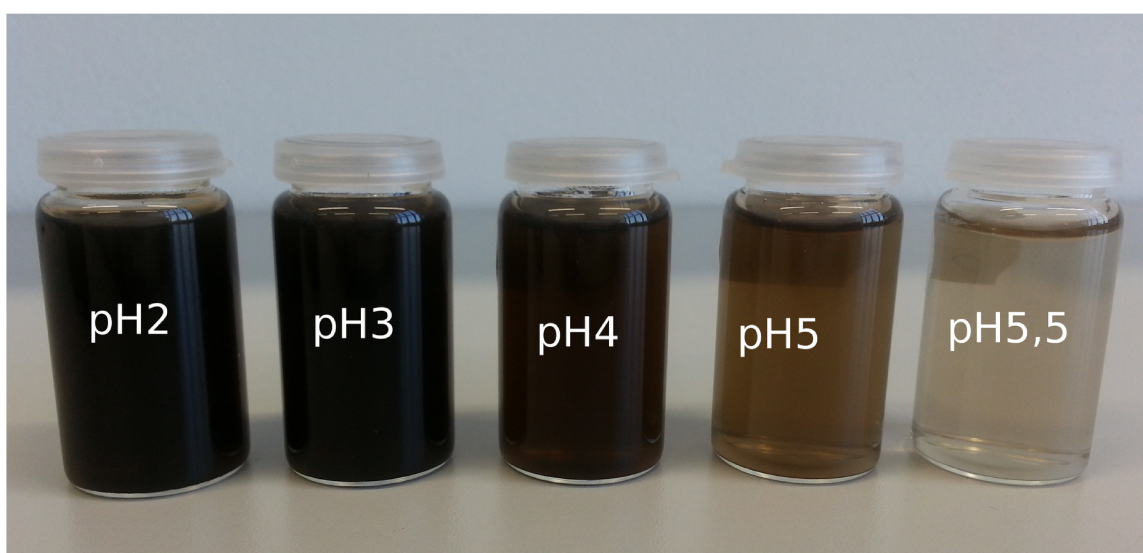

Fig. 6: Water dispersions of MCPs based on primary NPs of sample 1 obtained by peptization.

5.4 Modification

Stable dispersions were obtained by peptization of MCPs based on primary NPs of samples 1, 2 and 3 at low pH (approximately 1,5 - 4,5). Further modification of MCPs surface by citric acid and Al_2O_3 NPs was performed for NPs of sample 1, as it revealed the best heating performance. To this end, 0,001 g of citric acid was used per 10 ml dispersion, and Al_2O_3 NPs were used at 1:1 mass ratio to iron oxide content. After mixing of solution and modification agents, ultrasonic treatment was applied for 15 minutes. The Al_2O_3 modified MCPs were further subjected to dialysis treatment by sealing inside a dialysis tubing cellulose membrane, which was immersed in demineralized water for several weeks while slow continuous stirring.

6 SAMPLE ANALYSIS

In this section, methods and instruments used to determine the physical properties of samples will be specified.

6.1 LDV

Malvern Zetasizer Nano ZS was used to determine the zeta potential of the particles. Smoluchowski approximation was used in the Henry equation instead of Henry's function. Each sample was measured three times at 25 °C using 10 to 100 runs per measurement.

6.2 DLS

Hydrodynamic size of the particles was measured with Zetasizer Nano ZS (Malvern Instruments). Each of the samples was measured three times at 25 °C using 12 to 15 runs per measurement.

6.3 ED-XRF

ARL Quant'X ED-XRF Analyzer, Thermo Scientific was used to determine the iron oxide and Fe content in the sample.

6.4 SLP

In the current study, a home-made measuring system was used to determine the SLP of the samples. It consists of a signal generator (Agilent 33521A), RF broadband amplifier (AR RF/Microwave Instrumentation 800A3A), induction coil (90 mm diameter), interchangeable capacitors and measuring units for temperature and magnetic field sensing. The measurements were carried out at AMF with frequency of 1048 kHz and amplitude of 5,8 kA/m. Each sample was measured at least 3 times. Initial temperature was always set to room temperature (approximately 20 °C). Microsoft Excel software was used to process the data acquired. The samples were measured in low-viscosity media (water) and high-viscosity media (agar). The agar dispersions were prepared by adding 0,007 g of agar powder to 2 g of aqueous dispersions and heating to boiling temperature while stirring. Then the samples were placed in the fridge to immediately create a gel-like structure.

6.5 TEM

Samples were measured by TEM in the form of dried powders. JEOL JEM – 2100F was used to carry out the measurment. Particle size distribution data were obtained from measurements of 250 NPs at least, from TEM images with different magnification.

6.6   VSM

The magnetostatic properties were measured by a vibrating sample magnetometer Lake Shore 7407 at room temperature in an air atmosphere in a magnetic field of up to 10 kOe.

7 RESULTS

Results of measurements conducted on various samples will be provided and represented grafically in this section.

7.1 TEM

TEM was used to determine the morphology of primary NPs (cores) obtained. The MCPs structures were not possible to observe with TEM, as they were probably damaged while sample preparation for TEM. Figures 7, 8 and 9 depict TEM of primary NPs of samples 1, 2 and 3 respectively, along with the particle size distribution histograms.

(a)   **(b)**
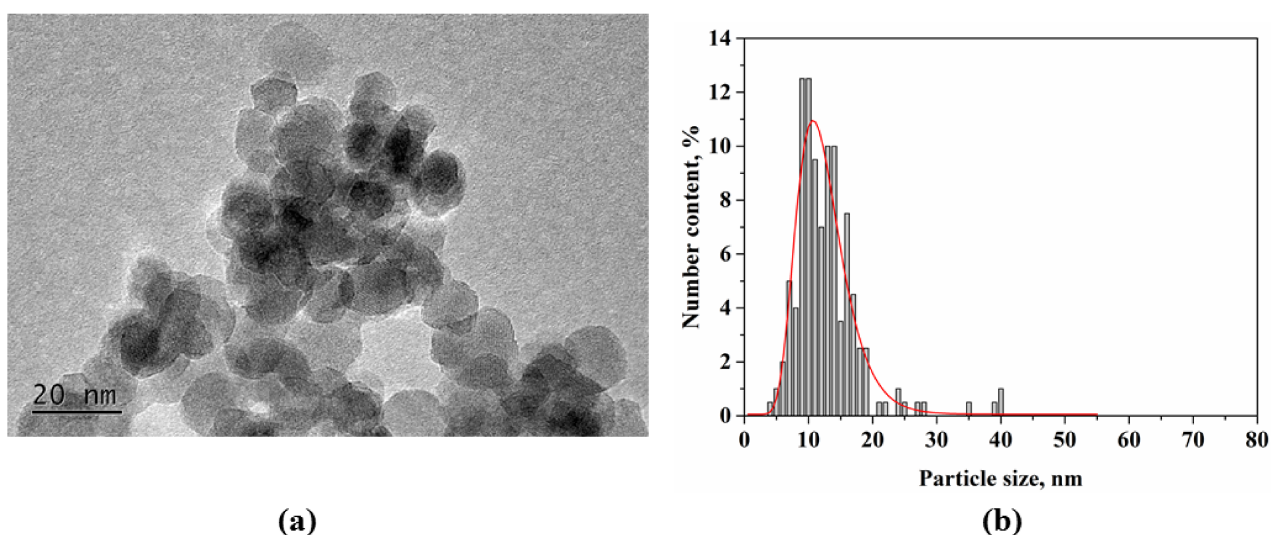
Fig. 7: TEM results of sample 1: (a) TEM image of primary NPs, (b) size distribution histogram.

(a)   **(b)**
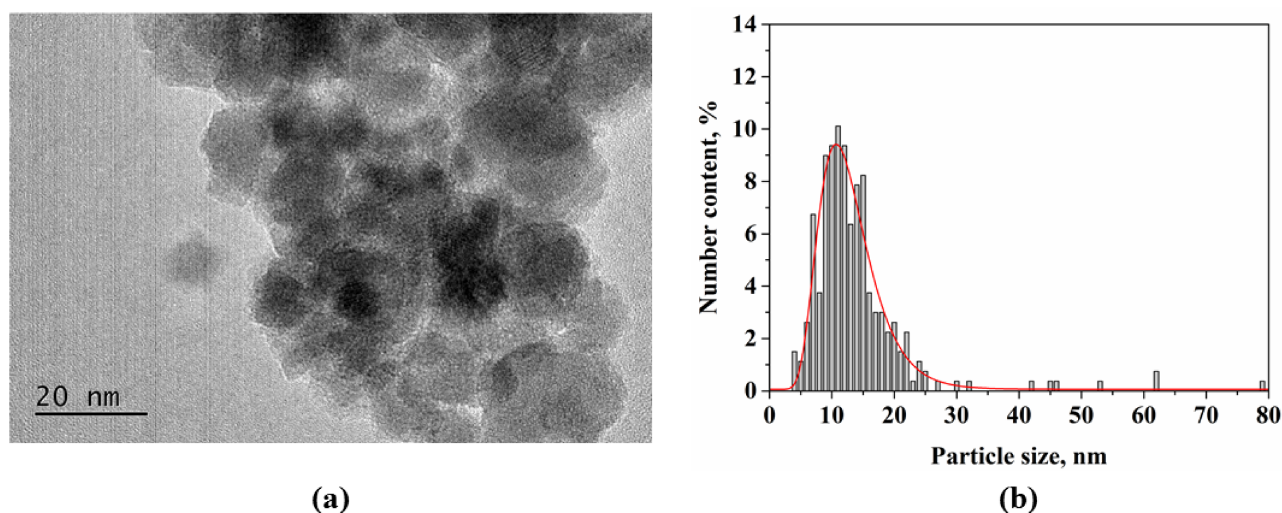
Fig. 8: TEM results of sample 2: (a) TEM image of primary NPs, (b) size distribution histogram.
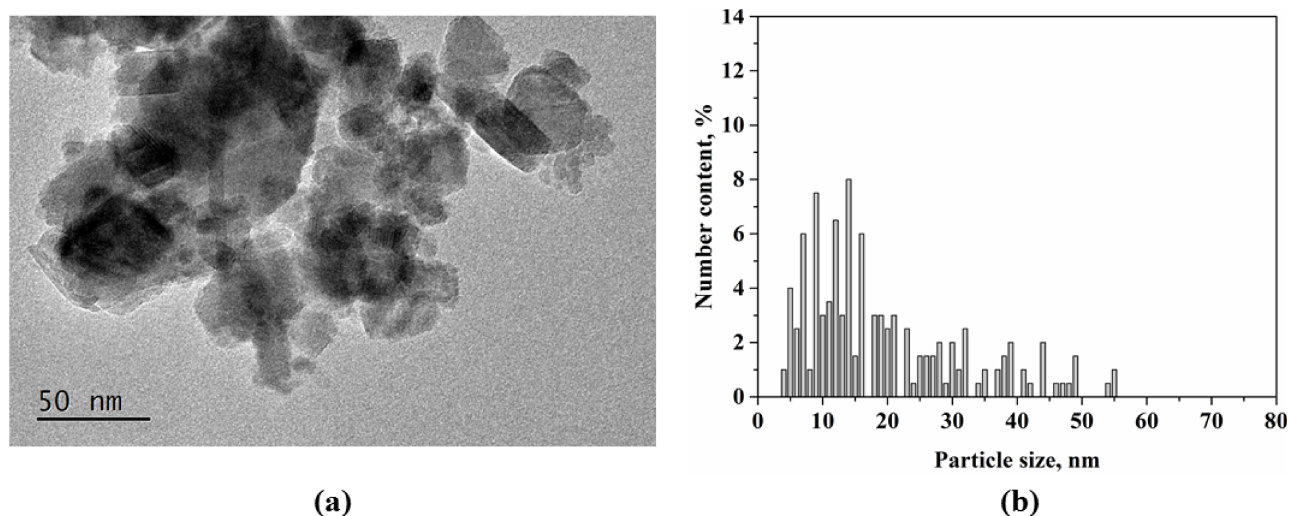
Fig. 9: TEM results of sample 3: (a) TEM image of primary NPs, (b) size distribution histogram.

7.2 DLS and LDV measurements

DLS and LDV measurements were done for all water dispersions. The obtained characteristics are MCPs hydrodynamic size, polydispersity index (PdI) and zeta pontential. The data are represented in table 2 and 3.

Table 2: DLS and LDV data for water dispersions of bare and surface modified MCPs on the base of sample 1

Sample		Hydrodynamic size [nm]	PdI	Zeta potential [mV]
Sample 1	S1_pH2	86	0,1	45±2
	S1_pH3	134	0,1	40±2
	S1_pH4	162	0,1	41±2
	S1_pH5	191	0,1	33±4
	S1_pH2_cit.acid	70	0,2	-21±5
	S1_pH2_Al$_2$O$_3$	91	0,2	46±2
	S1_pH3_Al$_2$O$_3$	101	0,2	43±0,3
	S1_pH4_Al$_2$O$_3$	114	0,2	47±0,2

Table 3: DLS and LDV data for water dispersions on the base of samples 2 and 3

Sample		Hydrodynamic size [nm]	PdI	Zeta potential [mV]
Sample 2	S2_pH2	55; 180 average: 131	0,3	49±3
	S2_pH3	93	0,2	40±5
	S2_pH4	109	0,2	44±3
Sample 3	S3_pH2	75; 253 average: 137	0,3	53±9
	S3_pH3	77	0,2	44±3

7.3 VSM measurements

VSM measuments were conducted on water dispersions on the base of sample 1 representing MCPs of various hydrodynamic sizes. Since the samples 2 and 3 display great variability in other characteristics, they are not suitable for further research and their magnetostatic properties were not measured. Coercivity (Hci) and saturation magnetization (M_S) are presented in table 4.

Table 4: VSM data for the MCPs on the base of sample 1

Sample		Hci [Oe]	M_s [emu/g(FeOx)]
Sample 1	S1_pH2	0,2	40
	S1_pH3	0,5	40
	S1_pH4	0,9	40
	S1_pH5	7,8	40
	S1_pH2_cit.acid	0,2	40

7.4 Iron oxide concentration and SLP measurement

Iron oxide concentration in dispersions are presented alongside with SLP of water and agar dispersions in tables 5, 6, 7 and 8.

Table 5: Iron oxide concentration and SLP of water and agar dispersions based on sample 1

Sample		Concentration of iron oxide in dispersion [wt. %]	SLP in water [W/g(Fe)]	SLP in agar [W/g(Fe)]
Sample 1	S1_pH2	0,037	42±5	28±6
	S1_pH3	0,036	25±4	23±4
	S1_pH4	0,025	8±3	9±3
	S1_pH5	0,012	0	0

Table 6: Iron oxide concentration and SLP of water and agar dispersions on the base of samples 2 and 3

Sample		Concentration of iron oxide in dispersion [wt.%]	SLP in water [W/g(Fe)]	SLP in agar [W/g(Fe)]
Sample 2	S2_pH2	0,5	46±9	44±17
	S2_pH3	0,3	49±6	36±5
	S2_pH4	0,2	38±8	28±11
Sample 3	S3_pH2	0,02	54±33	44±33
	S3_pH3	0,05	54±51	24±19

Table 7: SLP of water and agar dispersions of bare and citric acid modified MCPs with various concentrations of iron oxide

Sample	Concentration of iron oxide in dispersion [wt.%]	SLP in water [W/g(Fe)]	SLP in agar [W/g(Fe)]
S1_pH2	0,06	42±5	28±6
	0,2	44±2	29±3
	1	48±1	21±1
S1_pH2_cit.acid	0,06	61±3	54±2
	0,2	52±1	48±4
	1	51±2	43±1
	5	46±1	41±3
	6	40±4	32±4

Table 8: Iron oxide concentration and SLP of water and agar dispersions of Al_2O_3 modified MCPs based on sample 1

Sample	Concentration of iron oxide in dispersion [wt.%]	SLP in water [W/g(Fe)]	SLP in agar [W/g(Fe)]
S1_pH2_Al$_2$O$_3$	0,3	52±1	39±1
S1_pH3_Al$_2$O$_3$	0,2	45±1	33±3
S1_pH4_Al$_2$O$_3$	0,1	28±4	55±4

8 DISCUSSION

8.1 Influence of primary NPs morphology on magneto-structural properties and heating efficiency of MCPs on their base

Three synthesis approaches were used in order to obtain different morphologies of primary NPs. As is apparent from TEM images (Fig. 7, 8 and 9), sample 1 consists of uniform, spherical NPs of approximately 13 nm in diameter. PdI of this sample is 0,3. The primary NPs in sample 2 have broder size distribution with PdI of 0,4. NPs of various diameter are clearly seen, but the shape still remains spherical and average NPs diametr is 13 nm. Primary NPs of sample 3 are far larger in diameter than NPs of other samples, and there is no uniformity in shape. Aside from spherical NPs, rod-like and cubic-like NPs appear.

DLS and LDV measurements of water dispersions of MCPs on the base of samples 1,2 and 3 (Tables 2 and 3) show no significant shift in zeta potential between different morphologies of primary NPs, which is not surprising as all the dispersions remain stable. However, great difference is apparent in hydrodynamic size of the MCPs. While in sample 1 the peptization at certain pH gives dispersions of MCPs with quite narrow size distribution, samples 2 and 3 display broad size distribution, sometimes even two peaks of very low (approximately 60 nm) and high (approximately 200 nm) diameters can be observed. PdI of hydrodynamic size for samples 2 and 3 is therefore higher than the one for sample 1, which causes low reproducibility of other experimental data.

SLP measurements (Tables 5 and 6) were conducted on water and agar dispersions on the base of all types of primary NPs. According to [29], the Néel relaxation losses, and consequently the overall heating efficiency, should be incresed by higher shape anisotropy of MCPs cores. This could be an explanation of better SLP results for sample 2 compared to sample 1. As shape anisotropy of primary NPs of sample 2 can be considered higher than for sample 1, the Néel relaxation losses are expected to be higher. The SLP results of sample 3 are very inconsistent and almost irreproducible, therefore the study of these MCPs would not bring any contribution to the issue of this thesis. The low reproducibility must be taken into account when evaluating the results of sample 2 as well. The correlation found between shape anisotropy and Néel relaxation losses can be purely coincidental, which is why sample 2 will not be considered in the next sections either. In order to study the shape anisotropy influence, more experiments are needed, perhaps with non-spherical primary NPs and low polydispersity in order to ensure reproducible results.

8.2 Electrostatically stabilized MCPs - the influence of hydrodynamic size on heating efficiency

Acidification of primary NPs after synthesis by diluted HCl was performed in order to achieve peptization of MCPs, yielding stable dispersions. This happens due to protolithic reaction between amphoteric magnetite surface and H^+ ions of HCl, which follows the equation: $Fe\text{-}OH + H^+ \leftrightarrow Fe\text{-}OH_2^+$.

In previous studies it has been confirmed, that size fractionation of MNPs is essential for SLP enhancement [30,31]. In the current work size fractionation was achieved by collecting the supernatants at various pH values. As is shown in table 2, the MCPs in dispersion have narrow size distribution and the hydrodynamic size increases with the increase of pH. However at pH about 5-5,5, the peptization stops. Therefore, isoelectric point can be assumed to be in this range of pH.
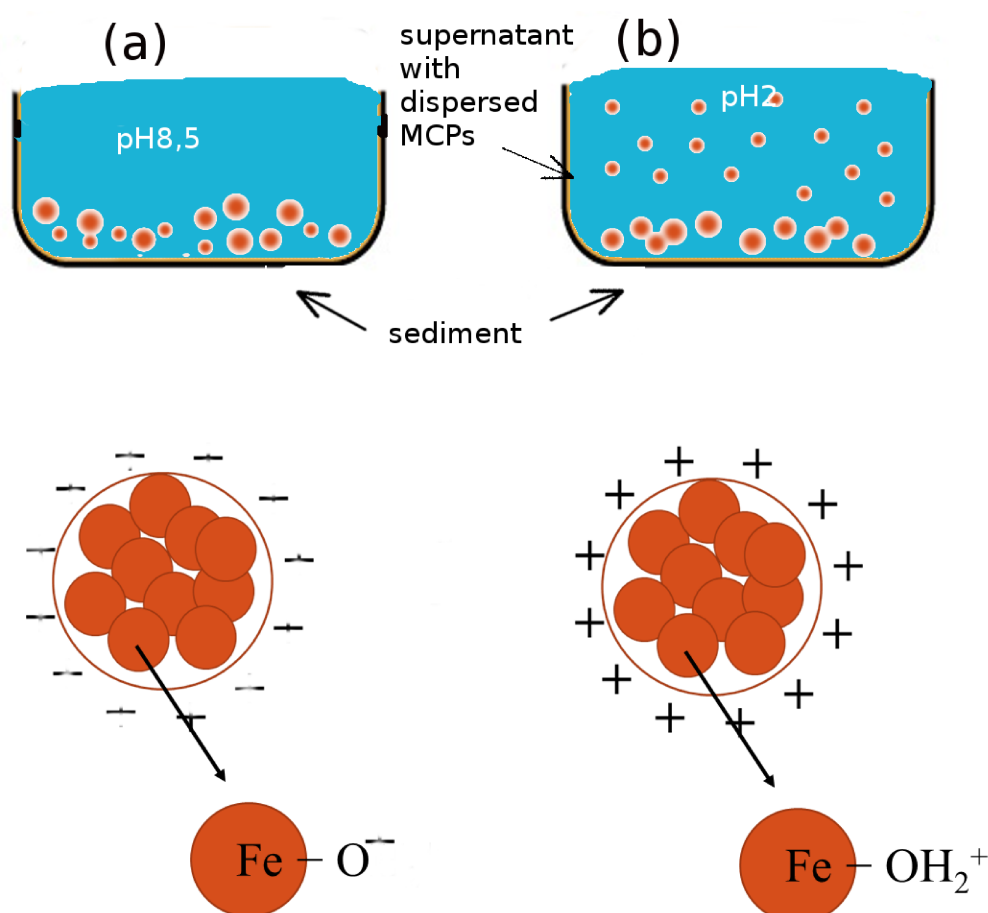
Fig. 10: Scheme of protonization and peptization of iron oxide MCPs of certain hydrodynamic size; (a) aggregated NPs after synthesis in slightly alkaline media, (b) peptization of MCPs after HCl treatment in acidic media.

A significant decline of SLP in water was observed for MCPs of bigger hydrodynamic size, despite the lack of change in magnetization saturation. In order to determine the contribution of Brown and Néel relaxations, SLP measurements were conducted also in agar dispersion. Agar, being high-viscosity medium, suppresses the Brown relaxation, leaving the Néel relaxation unchanged, as it is not viscosity-dependent [3]. The measurements of agar dispersions showed significantly lower heat outcomes, confirming the presence of Brown relaxation losses in water dispersions. They also display declining tendency with increse of MCPs hydrodynamic size. According to [29] , this can be explained by decrease of Néel relaxation time τ_0 with increase of MCPs size.

The obtained results were presented on the conference „16th Czech and Slovak Conference on Magnetism" and a manuscript was submitted to Acta Polonica, current status: accepted for publication.

8.3 Citric acid modified MCPs - interparticle interaction effect on heating efficiency

Citric acid modification changes the zeta potential of the MCPs (Table 2). Although zeta potential declined in number, the long-term stability of the dispersions rose comared to uncovered ones, and concentrated dispersions displayed good stability as well. However, the positive outcome of citric acid on stability was observed only for pH 2-2,5. In higher pH, the stability dropped rapidly, which apparently indicates the shift of MCPs isoelectric point from pH approximately 5,5 to pH between 2,5-3.
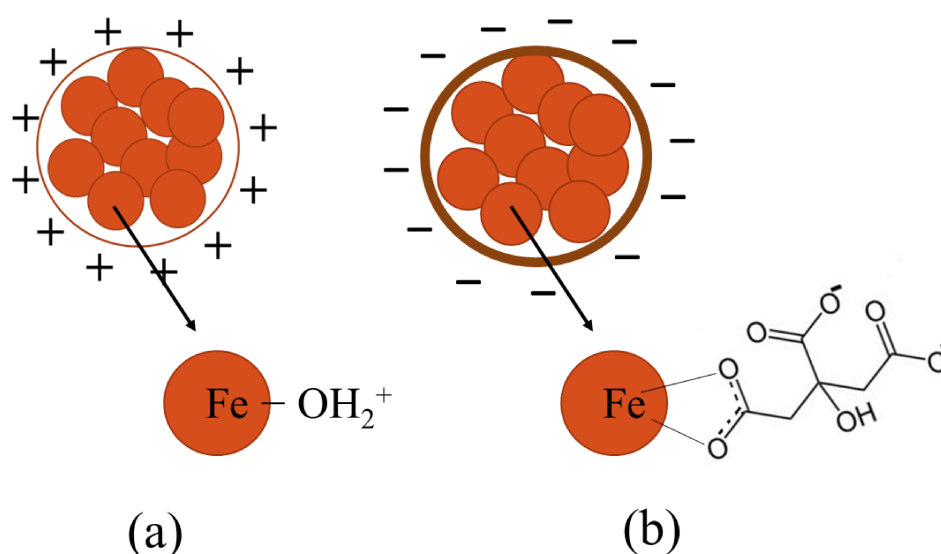
Fig. 11: Scheme of citric acid surface modification of MCPs, where (a) represents bare iron oxide MCP, and (b) represents citric acid coated MCP.

As is apparent from table 7, the citric acid coating enhances the SLP of MCPs. This can be explained by distancing of the MCPs, due to that their magnetic interactions are suppressed and dynamic hysteresis losses are higher.

To confirm this theory, concentration dependece of SLP was measured (Table 7). The citric acid coated MCPs were chosen due to their restrictive effect on MCPs proximity, and their positive influence on stability of dispersions with high concentration. In both bare (S1_pH2) and citric acid coated (S1_pH2_cit.acid) samples, the SLP drops slowly until concentration of 1 wt.% of iron oxide in dispersion. At higher concentration, only citric acid coated MCPs are stable. As is evident from table 7, SLP of both water and agar dispersions decreases with the increase of concentration. MCPs are getting closer with the increase of concentration, thus lowering the restriction effect of citric acid on multicore-to-multicore interactions, that deteriorate the heating efficiency.

As stated earlier, Brown relaxation is suppressed in agar matrix. Therefore, if we extract the SLP values for agar dispersions (solely Néel relaxation contribution to SLP) from the values of SLP for water dispersions (both Brown and Néel relaxation contributions to SLP), SLP due to Brown relaxation can be recieved. As can be seen from Fig. 12, the Néel relaxation losses drop significantly with the increase of concentration, whereas Brown relaxation losses remain almost constant. This leads to a conclusion that only Néel relaxation is affected by the multicore-to-multicore interactions.
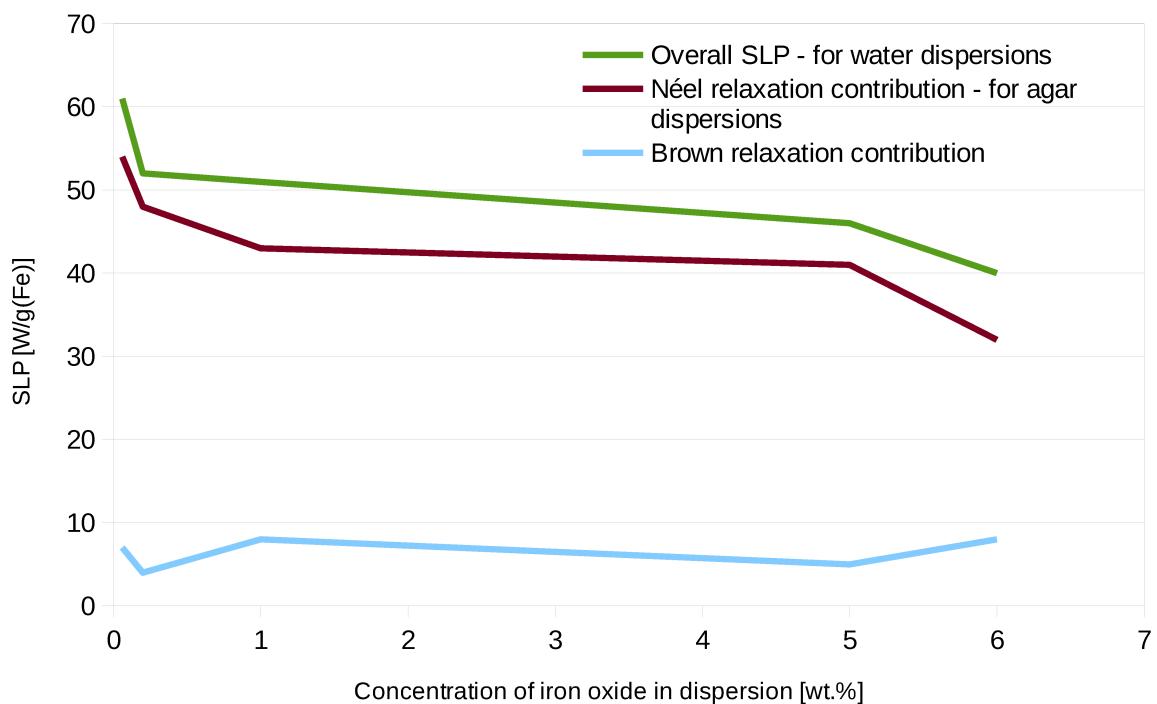

Fig. 12: Concentration dependence of SLP devided into Brown and Néel relaxation contributions for dispersions of citric acid surface modified MCPs

The obtained results were presented on the conference „ NANOCON 2016 " and are included in the proceedings of the conference that have been approved for indexing in the database Web of Science / Web of Knowledge (Thomson Reuters).

8.4 Al_2O_3 modified MCPs - significant effect on the dispersion stability and enhancement of heat outcome

The mechanism of Al_2O_3 haloing the MCPs is studied in [18], in which the findings suggest the Al_2O_3 NPs enclose iron oxide MCPs within some sort of a shell. In the current study, the Al_2O_3 modification resulted in MCPs of diameter of about 100 nm and narrow size distribution regardless the initial hydrodynamic size of MCPs before Al_2O_3 modification (Table 2). This can be ascribed to the effect of Al_2O_3 shell, that causes the iron oxide NPs within MCPs to pack more closely (Fig. 13). This enables the cores to have stronger magnetic interaction within the MCPs, i.e. both exchange interactions and dipole-dipole interactions. The later are assumed to be dominating interactions within bare MCPs of bigger hydrodynamic size. This suggestion is supported by higher SLP of Al_2O_3 modified MCPs compared to bare MNPs (Tables 5 and 8), that, according to theoretical model made by Ahrentorp et.al., 2015 [14], can be due to stronger magnetic interaction between the cores in Al_2O_3 modified MCPs. The Al_2O_3 shell serves as a multicore-to-multicore interaction restrictive agent, the same way the citric acid coating works. As the Al_2O_3 modified MCPs have almost the same hydrodynamic size, they show no significant difference of heat outcome in AMF (Fig. 14).
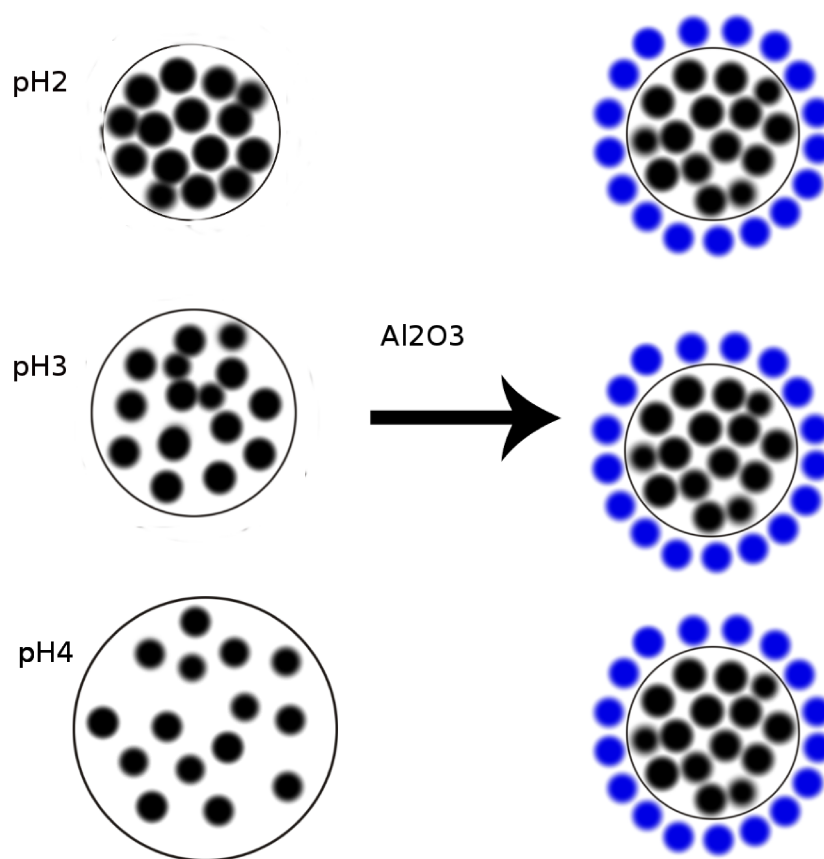
Fig. 13: Scheme of Al$_2$O$_3$ modification of iron oxide MCPs of various hydrodynamic size; black dots represent Fe$_3$O$_4$ cores of 13 nm in diameter, blue dots represent Al$_2$O$_3$ NPs of 13 nm in diameter.
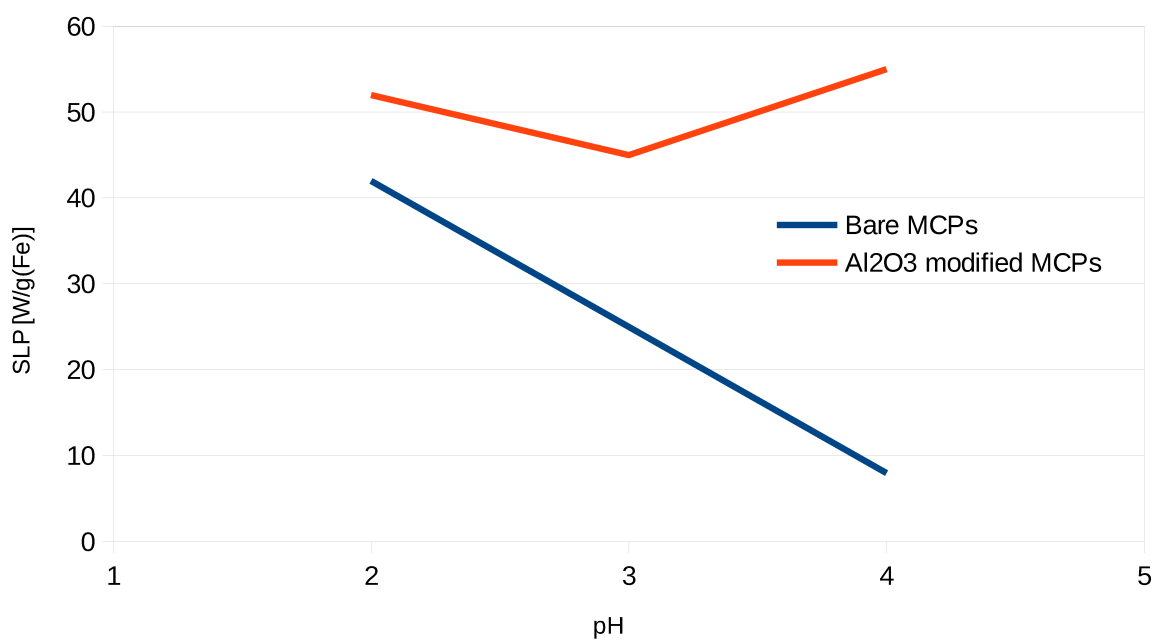

Fig. 14: Comparison of SLP of water dispersions of bare MNPs and Al$_2$O$_3$ surface modified MNPs on the base of sample 1

Another great contribution of Al_2O_3 modification is very good stabilization effect in high pH. According to Zubir et. al., 2015 [18], the stability and zeta potential of Al_2O_3 modified samples sustains at pH slightly above 6. This was proven in the current study by dialysis of the water dispersion of sample S1_pH2_Al_2O_3 until pH 6. The dispersion remained stable and kept the original hydrodynamic size, as well as the zeta potential. This was not observed in any other sample. The SLP values also remained the same as before dialysis. These results suggest strong non-covalent bonding among Al_2O_3 and MCPs of iron oxide, and their ensemble adopting the zeta potential and isoelectric point of Al_2O_3 NPs. Along with the pH being almost neutral and biocompatibility of both iron and aluminum oxides, the enhanced heat outcome makes the Al_2O_3 surface modified MCPs a promising mediator for magnetic hyperthermia treatment.

By all means, the Al_2O_3 haloing is a novel approach on NPs dispersion stabilization and deserves to be studied more profoundly in order to fully understand its complex impact on iron oxide magneto-structural properties.

CONCLUSION

The main objective of the thesis is to establish the correlation between magneto-structural parameters of magnetic iron oxide MCPs and magnetization dynamics in AFM. To this end, primary iron oxide NPs of different morphologies were prepared by coprecipitation of iron salts in an alkaline media. After that, MCPs on their base were prepared by acidification of the alkaline dispersion and peptization of supernatant containing MCPs of certain hydrodynamic size. These were in some cases further surface modified by either citric acid, or Al_2O_3 NPs.

The primary NPs' morphology and size polydispersity was established by TEM. Spherical primary NPs with polydispersity of 0,3 (sample 1), as well as spherical primary NPs with higher polydispersity (sample 2) and primary NPs variable in both shape and size (sample 3) were prepared. The MCPs on the base of sample 1 are the only ones to give reproducible outcomes in further measurements, therefore the study confines to these MCPs.

In order to improve the long-term stability of the MCPs dispersions, the MCPs surface was modified by citric acid. The long-term stability improved dramatically, especially in dispersions of high concentration. Unfortunately, the positive effect of citric acid coating occured only in dispersions of pH 1,5-2,5 and MCPs hydrodynamic size of 70 nm. The heat outcome in AMF is enhanced in comparison to bare MCPs. This is assumably due to restricted proximity of citric acid coated MCPs, that prevents magnetic multicore-to-multicore interactions and therefore enhances the Néel relaxation. This was confirmed by measurement of concentration dependence of SLP. As stated earlier, the stability of highly concentrated dispersions of citric acid coated MCPs makes them the most suitable for such experiment. The Néel relaxation contribution to overall SLP declines with the increase of concentration, but Brown relaxation contribution remains almost constant. Therefore, it can be assumed that citric acid coating indeed influences multicore-to-multicore magnetic interactions.

An alternative stabilization approach was performed by surface modification of iron oxide MCPs using Al_2O_3 NPs. The stabilization mechanism is rather different from conventional surfactants, as the bonds between the MCPs and Al_2O_3 are non-covalent. The so-called Al_2O_3 haloing has many interesting impacts on iron oxide MCPs structural properties, as well as on magnetization dynamics. The long-term stability of the dispersions was enhanced for any given pH. An important outcome is that the dispersion remained stable also after dialysis treatment until pH 6, which was not possible for any other sample in the current study. Interestingly, the size of the Al_2O_3 modified MCPs was about 100 nm regardles the original MCPs size. It is assumed that Al_2O_3 NPs modification causes the cores within an MCP to pack more closely. The Al_2O_3 modified MCPs also show higher heat

outcome than bare MCPs, which can be explained in similar way as in the case of citric acid surface modification.

To conclude, the most important findings of this thesis are the following:

- Non-uniformity of primary NPs morphology has negative effect on reproducibility of other measurement results.

- The long-term stability of MCPs dispersion with electrostatic stabilization is rather low in most cases, but can be enhanced by suitable surface modification, such as citric acid coating or Al_2O_3 NPs haloing.

- The coating also restrains multicore-to-multicore magnetic interactions and enhances the heating efficiency in AMF.

- Al_2O_3 NPs provide the dispersion with stability even at pH of 6.

It should be noted, that all the substances used were chosen with respect to biocompatibility of the system, and SLP measurements were conducted in low-intensity AMF, approved for magnetic hyperthermia treatment. The magneto-structural properties and high heating performance of Al_2O_3 modified MCPs make them a promising candidate for this application.

BIBLIOGRAPHY

[1] S. Chikazumi, Physics of Ferromagnetism, Oxford University Press Inc., New York, 1997.

[2] B.M. Moskowitz, Hitchhiker's Guide to Magnetism, Environ. Magn. Work. 279 (1991) 48. doi:10.1038/nm1005-1051.

[3] E.C. Abenojar, S. Wickramasinghe, J. Bas-Concepcion, A.C.S. Samia, Structural effects on the magnetic hyperthermia properties of iron oxide nanoparticles, Prog. Nat. Sci. Mater. Int. 26 (2016) 440–448. doi:10.1016/j.pnsc.2016.09.004.

[4] L. Suber, D. Peddis, Approaches to Synthesis and Characterisation of Spherical and Anisometric Metal Oxide Magnetic Nanomaterials, in: C.S. Kumar (Ed.), Magn. Nanomater., WILEY-VCH Verlag GmbH&Co.KGaA, Weinheim, 2009.

[5] J.M.D. Coey, Magnetism and Magnetic Materials, 1st ed., Cambridge University Press, New York, 2010.

[6] T. Miyazaki, H. Jin, The Physics of Ferromagnetism, Springer, Berlin, 2012.

[7] R.A. McCurrie, Ferromagnetic Materials: Structure and Properties, Academic Press Limited, London, 1994.

[8] I.S. Smolková, Iron oxide Nanoparticles and polymer composites on thereof for Magnetic Hyperthermia, Thomas Bata University in Zlín, 2014, Doctoral thesis.

[9] R.M. Cornell, U. Schwertmann, The Iron Oxides, 2nd ed., WILEY-VCH Verlag GmbH&Co.KGaA, Weinheim, 2003.

[10] N.N. Greenwood, A. Earnshaw, Chemistry of the Elements, 1st ed., Pergamon Pres plc, Oxford, 1984.

[11] G. Reiss, A. Hütten, Magnetic Nanoparticles, in: K.D. Sattler (Ed.), Handb. Nanophysics. Nanoparticles Quantum Dots, CRC Press, Boca Raton, 2009.

[12] K.Y. Yoon, Z. Xue, Y. Fei, J.H. Lee, V. Cheng, H.G. Bagaria, C. Huh, S.L. Bryant, S.D. Kong, V.W. Ngo, A.R. Rahmani, M. Ahmadian, C.J. Ellison, K.P. Johnston, Control of magnetite primary particle size in aqueous dispersions of nanoclusters for high magnetic susceptibilities, J. Colloid Interface Sci. 462 (2016) 359–367. doi:10.1016/j.jcis.2015.09.058.

[13] L. Gutiérrez, R. Costo, C. Grüttner, F. Westphal, N. Gehrke, D. Heinke, A. Fornara, Q. a Pankhurst, C. Johansson, M.P. Morales, Synthesis methods to prepare single- and multi-core iron oxide nanoparticles for biomedical applications, Dalt. Trans. (2015) 2943–2952. doi:10.1039/c4dt03013c.

[14] F. Ahrentorp, A. Astalan, J. Blomgren, C. Jonasson, E. Wetterskog, P. Svedlindh, A. Lak, F. Ludwig, L.J. Van Ijzendoorn, F. Westphal, C. Grüttner, N. Gehrke, S. Gustafsson, E. Olsson, C. Johansson, Effective particle magnetic moment of multi-core particles, J. Magn. Magn. Mater. 380 (2015) 221–226. doi:10.1016/j.jmmm.2014.09.070.

[15] D. Meyers, Surfaces, Interfaces and Colloids: Principles and Applications, 2nd ed., John Wiley and Sons, Inc., 1999.

[16] J.P. Novák et.al., Fyzikální chemie II, 1st ed., Vysoká škola chemicko-technologická v Praze, Praha, 2001.

[17] C.L. Altan, B. Gurten, R. Sadza, E. Yenigul, N.A.J.M. Sommerdijk, S. Bucak, Poly(acrylic acid)-directed synthesis of colloidally stable single domain magnetite nanoparticles via partial oxidation, J. Magn. Magn. Mater. 416 (2016) 366–372. doi:10.1016/j.jmmm.2016.05.009.

[18] M.N.M. Zubir, A. Badarudin, S.N. Kazi, M. Misran, A. Amiri, R. Sadri, S. Khalid, Experimental investigation on the use of highly charged nanoparticles to improve the stability of weakly charged colloidal system, J. Colloid Interface Sci. 454 (2015) 245–255. doi:10.1016/j.jcis.2015.05.019.

[19] H. Karimian, A.A. Babaluo, Halos mechanism in stabilizing of colloidal suspensions: Nanoparticle weight fraction and pH effects, J. Eur. Ceram. Soc. 27 (2007) 19–25. doi:10.1016/j.jeurceramsoc.2006.05.109.

[20] S. Dutz, R. Hergt, Magnetic particle hyperthermia-a promising tumour therapy?, Nanotechnology. 25 (2014). doi:10.1088/0957-4484/25/45/452001.

[21] M.G. Warner, C.L. Warner, R.S. Addleman, W. Yantasee, Magnetic Nanomaterials for Environment Applications, in: C.S. Kumar (Ed.), Magn. Nanomater., WILEY-VCH Verlag GmbH&Co.KGaA, Weinheim, 2009.

[22] S. Dutz, Are Magnetic Multicore Nanoparticles Promising Candidates for Biomedical Applications?, IEEE Trans. Magn. 52 (2016) 1–3. doi:10.1109/TMAG.2016.2570745.

[23] Y.K. Gun'ho, D.F. Brougham, Magnetic Nanomaterials as MRI Contrast Agents, in: C.S. Kumar (Ed.), Magn. Nanomater., WILEY-VCH Verlag GmbH&Co.KGaA, Weinheim, 2009.

[24] T.E. Thomas, S. Al Aani, D.L. Oatley-Radcliffe, P.M. Williams, N. Hilal, Laser Doppler Electrophoresis and Electro-osmotic Flow Mapping: a novel methodology for the determination of membrane surface zeta potential, J. Memb. Sci. 523 (2016) 524–532. doi:10.1016/j.memsci.2016.10.029.

[25] R. Xu, Progress in nanoparticles characterization: Sizing and zeta potential measurement, 6 (2008) 112–115. doi:10.1016/j.partic.2007.12.002.

[26] V. Helán, K. Walder, Rentgenová spektrometrie, in: 2nd ed., 2 THETA Český Těšín, Český Těšín, 1997.

[27] G. Cao, Nanostructures&Nanomaterials, Imperial College Press, London, 2004.

[28] S. Tumanski, Handbook of Magnetic Measurements, 1., CRC Press, Boca Raton, 2011.

[29] M. Harabech, J. Leliaert, A. Coene, G. Crevecoeur, D. Van Roost, L. Dupr, The effect of the magnetic nanoparticle's size dependence of the relaxation time constant on the specific loss

power of magnetic nanoparticle hyperthermia, J. Magn. Magn. Mater. 426 (2017) 206–210. doi:10.1016/j.jmmm.2016.11.079.

[30]   C. Wilhelm, C. Ménager, M. Curie, F. Gazeau, Size-Sorted Anionic Iron Oxide Nanomagnets as Colloidal Mediators for Magnetic Hyperthermia, (2007) 2628–2635. doi:10.1021/ja067457e.

[31]   T. Rheinländer, R. Kötitz, W. Weitschies, W. Semmler, Magnetic fractionation of magnetic fluids, J. Magn. Magn. Mater. 219 (2000) 219–228. doi:10.1016/S0304-8853(00)00439-X.

LIST OF ABBREVIATIONS

MCP   Multicore Particle

AMF   Alternating Magnetic Field

NP   Nanoparticle

MRI   Magnetic Resonance Imaging

SD   Single-domain

MD   Multi-domain

SPM   Superparamagnetic

LDV   Laser Doppler Velocimetry

DLS   Dynamic Light Scatterng

ED-XRF   Energy Dispersive X-ray Fluorescence Spectroscopy

SLP   Specific Loss Power

VSM   Vibrating Sample Magnetometry

MPI   Magnetic Particle Imaging

rpm   rotation per minute

PdI   Polydispersity index

Hci   Coercivity

M_S Magnetization saturation

LIST OF FIGURES

LIST OF TABLES